X-RAY AND TIMING PROPERTIES OF ANOMALOUS X-RAY PULSAR 1E 2259+586

A THESIS SUBMITTED TO
THE GRADUATE SCHOOL OF NATURAL AND APPLIED SCIENCES
OF
THE MIDDLE EAST TECHNICAL UNIVERSITY

BY

SİNEM ŞAŞMAZ MUŞ

IN PARTIAL FULFILLMENT OF THE REQUIREMENTS
FOR
THE DEGREE OF MASTER OF SCIENCE
IN
PHYSICS

AUGUST 2007

Approval of the Thesis

"X-RAY AND TIMING PROPERTIES OF ANOMALOUS X-RAY PULSAR 1E 2259+586"

Submitted by **SİNEM ŞAŞMAZ MUŞ** in partial fulfillment of the requirements for the degree of **Master of Science in Physics** by,

Prof. Dr. Canan Özgen
Dean, Graduate School of **Natural and Applied Sciences** _____

Prof. Dr. Sinan Bilikmen
Head of Department, **Physics** _____

Prof. Dr. Altan Baykal
Supervisor, **Physics Dept.,METU** _____

Assist. Prof. Dr. S. Çağdaş İnam
Co-Supervisor, **E.E. Dept., BAŞKENT U.** _____

Examining Committee Members:

Prof. Dr. Halil Kırbıyık(*)
Physics Dept., METU _____

Prof. Dr. Altan Baykal(**)
Physics Dept., METU _____

Prof. Dr. Ümit Kızıloğlu
Physics Dept., METU _____

Assoc. Prof. Dr. Berahitdin Albayrak
Astronomy and Space Sciences Dept., ANKARA U. _____

Assist. Prof. Dr. S. Çağdaş İnam
Electrical and Electronics Engineering Dept., BAŞKENT U. _____

Date: _____

(*) Head of Examining Committee
(**) Supervisor

I hereby declare that all information in this document has been obtained and presented in accordance with academic rules and ethical conduct. I also declare that, as required by these rules and conduct, I have fully cited and referenced all material and results that are not original to this work.

Name, Last Name : SİNEM ŞAŞMAZ MUŞ

Signature :

ABSTRACT

X-RAY AND TIMING PROPERTIES OF ANOMALOUS X-RAY PULSAR 1E 2259+586

MUŞ, SİNEM ŞAŞMAZ

M.S., Department of Physics

Supervisor: Prof. Dr. Altan Baykal

Co-Supervisor: Assist. Prof. Dr. S. Çağdaş İnam

August 2007, 78 pages

In this thesis, we present the spectral and timing variabilities of anomalous X-ray pulsar 1E 2259+586 observed with European Photon Imaging PN Camera (EPIC PN) on board X-ray Multi Mirror Mission (XMM), Proportional Counter Array (PCA) on board Rossi X-ray Timing Explorer (RXTE) and Advanced CCD Imaging Spectrometer (ACIS) on board Chandra X-ray Observatory.

We presented the results of spectral analysis of 2000 January 11 ACIS observation. Pulse phase spectroscopy was performed on two XMM observations before and after the outburst. Pulse profiles of two XMM observations before the outburst and three XMM observations after the outburst were studied. Results are consistent with the those presented by Patel et al. (2001) and Woods et al. (2004).

We searched for the spectral variations versus spin rate during the outburst. Long-term spectral, frequency and spin-down rate variations are presented between 1996 and 2006 including 98 RXTE and 4 XMM observations. However, except outburst

region (Woods et al. 2004) no significant spectral and spin rate variabilities were seen. Around the outburst region we confirmed the spectral hardening with increasing spin rate and flux.

Keywords: neutron stars, anomalous X-ray pulsars, 1E 2259+586, X-rays, burst, Chandra, XMM and RXTE spectral analysis, RXTE timing.

ÖZ

ANORMAL X-IŞIN ATARCASI 1E 2259+586'NIN X-IŞIN VE ZAMANLAMA ÖZELLİKLERİ

MUŞ, SİNEM ŞAŞMAZ
Yüksek Lisans, Fizik Bölümü
Tez Yöneticisi: Prof. Dr. Altan Baykal
Ortak Tez Yöneticisi: Assist. Prof. Dr. S. Çağdaş İnam

Ağustos 2007, 78 sayfa

Bu tezde XMM EPIC PN, RXTE PCA ve Chandra ACIS kamera ve detektörleri ile gözlemlenen anormal X-ışın atarcası 1E 2259+586'nın spektrel ve zamanlama değişkenlikleri sunulmaktadır.

11 Ocak 2000 tarihli ACIS gözleminin analiz sonuçlarını sunduk. Patlamadan önce ve sonra yapılan iki XMM gözleminin spektrel parametrelerini atım fazına göre inceledik. Patlamadan önceki iki XMM gözlemi ve sonraki üç XMM gözleminin atım profillerini çalıştık. Elde edilen sonuçlar Patel ve ark. (2001) ve Woods ve ark. (2004) tarafından bulunan sonuçlar ile uyumludur.

Patlama süresince spektrel parametrelerdeki değişimi yıldızın spin değişim hızına göre araştırdık. Uzun dönemli spektrel, frekans ve yavaşlama hızı değişimlerini 98 RXTE ve 4 XMM gözlemini içeren 1996 ve 2006 yılları arasında araştırdık. Fakat, daha önce yayınlanan (Woods et al. 2004) patlama zamanı hariç diğer zamanlarda hiçbir değişim bulamadık. Patlama sırasında, spin değişim hızında ve akıda artış ile

foton indeksin azaldığını doğruladık.

Anahtar Kelimeler: nötron yıldızları, anormal X-ışın atarcaları, 1E 2259+586, X-ışınları, patlama, Chandra, XMM ve RXTE spektrel analizleri, RXTE zamanlama.

ACKNOWLEDGMENTS

I would like to express my deepest gratitude to my supervisor, Prof. Dr. Altan Baykal for his sincerity, guidance, support and insight throughout my graduate study. I would like to thank my co-supervisor Assist. Prof Dr. S. Çağdaş İnam for his great effort, guidance and encouragement during this study.

I would like to thank Elif Beklen for helpful discussions, motivation, support and everything I learned from her during this study.

I would like to express my deepest thanks to my loving family for their continuous support and trust in me throughout my life.

I especially thank METU Aikido Dojo for their existence and the moments we shared together. I had the honor and pleasure of being a member of this community.

I thank my friends and colleagues in METU Astrophysics Group.

I acknowledge The Scientific and Technological Research Council of Turkey (TUBITAK) for their funds.

I am grateful to my husband, Köksal for his love, patience and every effort he made to stay at nights with me.

TABLE OF CONTENTS

LIST OF FIGURES

FIGURES

LIST OF TABLES

TABLES

LIST OF ABBREVIATIONS

ACIS Advanced CCD Imaging Spectrometer

ADAF Advection-Dominated Accretion Flow

ASM All Sky Monitor

AXPs Anomalous X-ray Pulsars

CIAO Chandra Interactive Analysis of Observations

EA Event Analyzer

EDS Experiment Data System

EPIC European Photon Imaging Camera

FOV Field of View

FWHM Full Width Half Maximum

GRBs Gamma-ray Bursts

HEASARC The High Energy Astrophysics Science Archive Research Center

HEG High Energy Grating

HETG High Energy Transmission Grating

HEXTE The High Energy X-ray Timing Experiment

HRC High Resolution Camera

LETG Low Energy Transmission Grating

MEG Medium Energy Grating

MJD Modified Julian Day

PCA Proportional Counter Array

PCU Proportional Counter Unit

RGS Reflection Grating Spectrometers

RXTE Rossi X-ray Timing Explorer

OM The Optical Monitor

SAA South Atlantic Anomaly

SAS Science Analysis System

SGRs Soft Gamma-ray Repeaters

SNR Supernova Remnant

XMM X-ray Multi Mirror Mission

CHAPTER 1

INTRODUCTION

Massive stars evolve to neutron stars after supernova explosion which is a result of endothermic fusion reaction of iron and nickel. If these objects have strong (i.e. $\geq 10^{12}$ Gauss) magnetic fields, and emit signals at the line of sight of us like a lighthouse, we called them pulsars. Pulsars are classified according to their emission mechanisms as rotation-powered or accretion-powered pulsars. In rotation-powered case, pulsar is considered to be a rotating magnetic dipole and the emission is the result of loss of the rotational kinetic energy due to magnetic dipole braking since braking causes spinning-down of the star. In accretion case, material is accreted either from a supernova remnant or a companion star. It is the gravitational potential energy of these material which gives the observed emission.

Anomalous X-ray pulsars (AXPs) and soft Gamma-ray repeaters (SGRs) differ from those known as rotation-powered and accretion-powered pulsars. There is no evidence for a companion or an accretion disk, and AXPs have softer X-ray spectra than those of accreting X-ray binaries. So, these differences made scientist to think about the emission mechanism of these objects. Owing to ambiguity of energy source, scientists have called them "anomalous". They have narrow range of spin periods about 6-12 seconds, are spinning-down with high rates (0.048 - 47 $\times 10^{-11}$ s s^{-1}, Woods & Thompson 2004), and X-ray luminosities are several orders of magnitude greater than those calculated from spin-down rates. There are seven confirmed AXPs, two candidate and only four SGRs. Since the discovery of AXP 1E 2259+586 emission mechanism has been discussed during a decade. Especially two models,

magnetar and fall-back disk have been the most acceptable models and currently the debate over the hypothesis is continuing with the more applicability of magnetar model.

1.1 Soft Gamma-ray Repeaters and Anomalous X-ray Pulsars

The detection of a burst from SGR 1806-20 on 1979 January 7 (Laros et al. 1986) leads to a new discussion continuing over two decades among astrophysicists. Three of these objects were also detected within the first three months of 1979 during the observations of gamma-ray bursts (GRBs). Unlike GRBs, SGRs show repetitious bursts of soft gamma-rays / hard X-rays, and have softer spectra than in GRBs. Their bursts can reach up to 10^{45} ergs s^{-1} (Golenetskii et al. 1984). Using the observations of SGR 1806-20, no correlation between burst energy and waiting time was found which implies a different mechanism than rapid bursters' (Laros et al. 1987). They show super-Eddington luminosity spikes with short durations (Kouveliotou et al. 2003), persistent X-ray emission with periods in the range of 5 - 8 seconds and rapid spin-down (Woods & Thompson 2004). Also X-ray pulse profile changes have been observed in these objects during their burst activities (Gögüş et al. 2002). Their association with supernova remnants (SNR) has led people to think SGRs are young neutron stars. Theories such as merger of two white dwarfs (Paczynski 1990), accretion onto the neutron star via accretion disk or fall-back disk (van Paradijs et al. 1995; Chatterjee, Hernquist, Narayan 2000; Alpar 2001), decay of a high magnetic field (Duncan & Thompson 1992) have been invoked to explain the nature of these objects. Currently there are four known SGRs.

First AXP was discovered with the first imaging X-ray telescope of NASA, Einstein X-ray Observatory, by Fahlman & Gregory in 1981. This object, 1E 2259+586, also has high luminosity than calculated from spin-down, no optical counterpart and softer spectrum than those of X-ray binary systems. Current search for the other counterparts of emission is being held (Hulleman et al. 2001; Tam et al. 2004). In

the following years, number of confirmed AXPs reached seven and two candidate was also proposed. Summary of recent observations of SGRs and AXPs can be seen from Tables 3.1-3.13. Generally, spectra of AXPs is fitted to a power law plus black-body model modified by interstellar absorption and, for SGRs this model and single power-law model for some sources give good fits. Bursts have been observed from these objects after a long time of their discovery (Gavriil et al. 2002; Kaspi et al. 2003). Also flux variability of these objects have been discovered although some of them have not shown burst activity. Recent years glitches have been observed from 1E 2259+586 at the time of an outburst with accompanying radiative changes and 1RXS J170849.0-400910 (Kaspi et al. 2003, Woods et al. 2004, Kaspi et al. 2000, Kaspi & Gavriil 2003, DallOsso et al. 2003).

CHAPTER 2

MODELS

2.0.1 Magnetar Model

Since the bursts similar to soft Gamma ray repeaters' bursts have been detected in AXPs, magnetar model is in great consider. Because SGRs and AXPs have similar period (P), spin-down rate ($\dot{P}$), and X-ray luminosity (L_x) values in the quiescent states of SGRs. Also, positive correlation between the hardness of the high energy component and spin-down rate shows a continuity within these sources (Marsden & White 2001). The major difference between AXPs and SGRs was the burst phenomenon of SGRs. Magnetar model was introduced to explain the physics of SGRs in 1992 by Robert Duncan and Christopher Thompson (Duncan & Thompson 1992). They attempted to explain SGRs as one type of magnetars and how these high-field neutron stars can form (Duncan & Thompson 1992; Thompson & Duncan 1993; Thompson & Duncan 1995). They proposed convective motions in a supernova core as the source of strong magnetic fields of neutron stars under some conditions. Dynamo mechanism as a generation of magnetic fields was firstly mentioned by Flowers & Ruderman (1977). As there was no known mechanism to drive the relative motion of charged fluid which generates the magnetic field in 1977 they considered fossil field or field generated at birth as the mechanism.

According to the magnetar model SGRs and AXPs have magnetic fields stronger than the quantum electro dynamical value which means cyclotron energy is compa-

rable with the electron's rest mass energy

$$\mathrm{B_{QED}} = \frac{\mathrm{m_e^2 c^3}}{\mathrm{e\hbar}} \approx 4.4 \times 10^{13}\ \mathrm{Gauss}. \tag{2.1}$$

where m_e and e are the rest mass and charge of the electron. External magnetic energy has to be the dominant energy source rather than rotational energy on a time scale,

$$\mathrm{t_{mag}} = 400 \left(\frac{\mathrm{B_{dipole}}}{10\mathrm{B_{QED}}} \right)^{-4} \tag{2.2}$$

and this is the essential difference between pulsars and magnetars (Thompson & Duncan 1995). Dipole field inferred from the spin-down rate is about 10^{14-15} Gauss. But recently some radio pulsars with dipole magnetic fields about 10^{14} G have been discovered (McLaughlin et al. 2003; Camilo et al. 2000). Therefore, the fundamental difference observed between these high field pulsars and magnetars is attributed to the internal field strength (Thompson et.al. 2002).

Several mechanisms have been invoked for the generation of persistent emission with an order of 10^{35} erg s^{-1} from SGRs and AXPs. Twisted magnetic field inside the star which is also strong enough to twist up the external magnetic field via subsurface motions is one of the hypothesis. This field is the source of currents which are responsible for the non-thermal persistent emission from active burst sources with a decaying time of 10-100 years (Thompson 2000). Twisted field bundle has a current,

$$\mathrm{I} \cong \left(\frac{\theta_{\mathrm{max}} \Phi \mathrm{c}}{8\pi \mathrm{L}} \right) \tag{2.3}$$

where Φ and L are the magnetic flux and length of the bundle. θ_{max} is the strain which cracks the crust. Thompson et al. (2000) suggest that the surface temperature of these sources is enough to feed the current via thermionic emission of ions and electrons. These particles can impact and heat the surface. But electrons can also be accelerated to the higher energies and Comptonized thermal X-ray photons can be released. So, energy dissipation of the current flow is,

$$\mathrm{L_X} = 3 \times 10^{35} \left(\frac{\theta_{\mathrm{max}} \mathrm{A}}{\mathrm{Z}} \right) \left(\frac{\mathrm{B_{NS}}}{10\mathrm{B_{QED}}} \right) \left(\frac{\mathrm{L}}{\mathrm{R_{NS}}} \right)^{-1} \left(\frac{\mathrm{a}}{0.5\ \mathrm{km}} \right)^{2} \mathrm{erg\ s^{-1}} \tag{2.4}$$

A and Z are the mass and charge of the ion and a is the length of the fracture. Second mechanism is the ambipolar diffusion of charged particles. It means the drift of

magnetic field and charged particles relative to the neutrons through the core and release of magnetic energy via friction or β reactions (Goldreich & Reisenegger 1992; Thompson & Duncan 1996). Ohmic decay occurs as a result of the resistivity of the plasma which is important in the small length scales. The final suggested mechanism is the Hall drift which is caused by the current flows through a magnetized plasma. Hall effect does not dissipate magnetic energy because the electric field generated by the current flows in the presence of a magnetic field is perpendicular to the current density which makes the magnetic energy constant (Goldreich & Reisenegger 1992). But it transports the short wavelength (shorter than local scale height) Hall drift waves which carry the magnetic energy to the outer crust where they can dissipated by the Ohmic decay (Thompson & Duncan 1996).

The other phenomena that must be explained is the burst mechanism seen all of the SGRs and some of the AXPs. Rearrangement (via an interchange instability or reconnection) of the magnetic field and cracking of the crust is suggested as an explanation for SGR bursts. According to Thompson and Duncan (1995) diffusion of the magnetic field inside the interior of the star produces a rearrangement of the field via the displacement of the external magnetic field lines which are anchored to the surface and generates a pair fireball in the magnetosphere of the star caused by the Alfven waves released directly into the magnetosphere. According to the model, radiation from this fireball is the reason of the observed bursts. Thomson and Duncan conjecture the dipole field of the SGR 0526-66 with a magnetic flux radius of Δ R as

$$\mathrm{B_{dipole}} > 2 \times 10^{14} \left(\frac{\mathrm{E_{fireball}}}{10^{44}\ \mathrm{erg}}\right)^{1/2} \left(\frac{\Delta \mathrm{R}}{10\ \mathrm{km}}\right)^{-3/2} \left(\frac{1+\Delta \mathrm{R}/\mathrm{R_{NS}}}{2}\right)^{3} \mathrm{G} \qquad (2.5)$$

where $\mathrm{E_{fireball}}$ is the burst energy trapped in the closed magnetic field lines. This field is bigger of the order of 10^2 than a typical pulsar field by recourse to the assumption of the energy released in the soft tail of the 1979 March 5 burst arises from the pair fireball. Also they explained the hyper-Eddington luminosity of this source as a degradation of the scattering cross-section through the confined plasma below the Thomson cross-section value, allowing to the such high luminosities. For less energetic bursts, they propose the cracking of the crust by ambipolar diffusion and Hall

drift. The field in the crust estimated for cracking the crust is,

$$\mathrm{B_{crust}} \approx 1 \text{ x } 10^{15} \left(\frac{\mathrm{E_{SGR}}}{10^{41} \text{ erg}} \right)^{-1/2} \left(\frac{\mathrm{l}}{1 \text{ km}} \right) \left(\frac{\theta_{\max}}{10^{-3}} \right) \text{ G} \tag{2.6}$$

l is the length of the fracture and θ_{max} is the strain which cracks the crust. This disturbance also changes the positions of the field lines attached to the fracture region and gives rise to Alfven pulse as explained but less energetic one.

2.0.2 Fall-Back Disk Model

Various scenarios have been proposed like low mass companion (Mereghetti & Stella 1995), disrupted binary companion (van Paradijs et al. 1995), and magnetar model to explain emission mechanisms of AXPs. Another mechanism proposed is the fall-back disk for the case in which the matter from the supernova explosion cannot be ejected perfectly and falls back to the neutron star because of the gravitational field of the star and a disk forms when material has sufficient angular momentum (Chatterjee, Hernquist, Narayan 2000; Alpar 2001). In this scenario, accretion is time dependent. So, the observed spin-down is explained by a diminishing accretion rate (Chatterjee et al. 2000), and the observed X-ray emission is explained as a result of the accreting material onto the star accompanied with optical/IR emission from the disk. When the accretion stops the system switches to the ordinary pulsar phase. The magnetic field range is in the conventional pulsar range ($\sim 10^{12}$ G) in contrast with the magnetar model. This means that the observed differences between AXPs, SGRs and radio pulsars come from different parameters related to the accretion rate. The location of the magnetospheric radius with respect to the light cylinder and the corotation radius defines the effectiveness of the disk on neutron star. The motion of the accreting material is dominated with the magnetic field of the star. The radius of this region is called magnetospheric radius ($\mathrm{R_m}$). Light cylinder is the radius at which the corotation speed is comparable with the speed of light. The material in the disk corotates with the star if it is located on the corotation radius (Shapiro & Teukolsky 1983). If the magnetospheric radius is greater than the light cylinder radius, disk evolves independently from the star. So, magnetosphere location relative to the light

cylinder determines whether disk interacts with the star or not. If the disk interacts with the star, corotation radius determines how it interacts. When the magnetosphere of the star is beyond the corotation radius at which the angular rotation frequency of the star is greater than the Keplerian frequency at R_m, this phase is called the 'propeller phase' because the centrifugal forces prevent the accretion onto the neutron star, and owing to the angular momentum transfer to the disk star will spin down. Lacking of the falling matter onto the surface of the star leads to a significantly low X-ray luminosities. As neutron star spins down, angular rotation frequency of the star decreases to the Keplerian frequency of the disk at the magnetospheric radius. This phase is called the 'tracking phase' and the star is X-ray bright. Other phase of the accretion is advection-dominated accretion flow (ADAF). According to the theory, star is observed as AXP when between the transition from propeller to tracking ($t = t_{trans}$) and two times the transition to the ADAF phase ($t = 2t_{ADAF}$) which corresponds to the accretion death time (Figure 2.1). During the transition time to the ADAF, luminosity falls to the 1% of the Eddington luminosity. Thus, the theory explains the narrow period clustering of the AXPs via the disk-magnetosphere interactions. Also, observed Optical/IR emission is found an explanation in the theory as the emission or reprocessing of X-ray irradiation from the disk (Hulleman et.al. 2000). But according to Li & Wang (2000) rotation rate of the accreting material will be reduced by the advection which leads to decrease in corotation radius while the magnetospheric radius slightly changes. This causes the magnetospheric radius to be greater than the corotation radius and return to the propeller phase again which means the period clustering of the AXPs and SGRs cannot be obtained from the accretion. Another trouble is that the theory has difficulty in grasping the large pulse fraction of the optical pulsations and burst mechanism (Kern & Martin 2002; Chatterjee, Hernquist, Narayan 2000). In order to overcome this intricacy, Eksi & Alpar (2003) proposed a hybrid model in which the star has a dipole field with a conventional pulsar magnetic field interacting with the disk and surface magnetic fields with higher multipoles. But the detailed derivation of the theory has not been done yet.

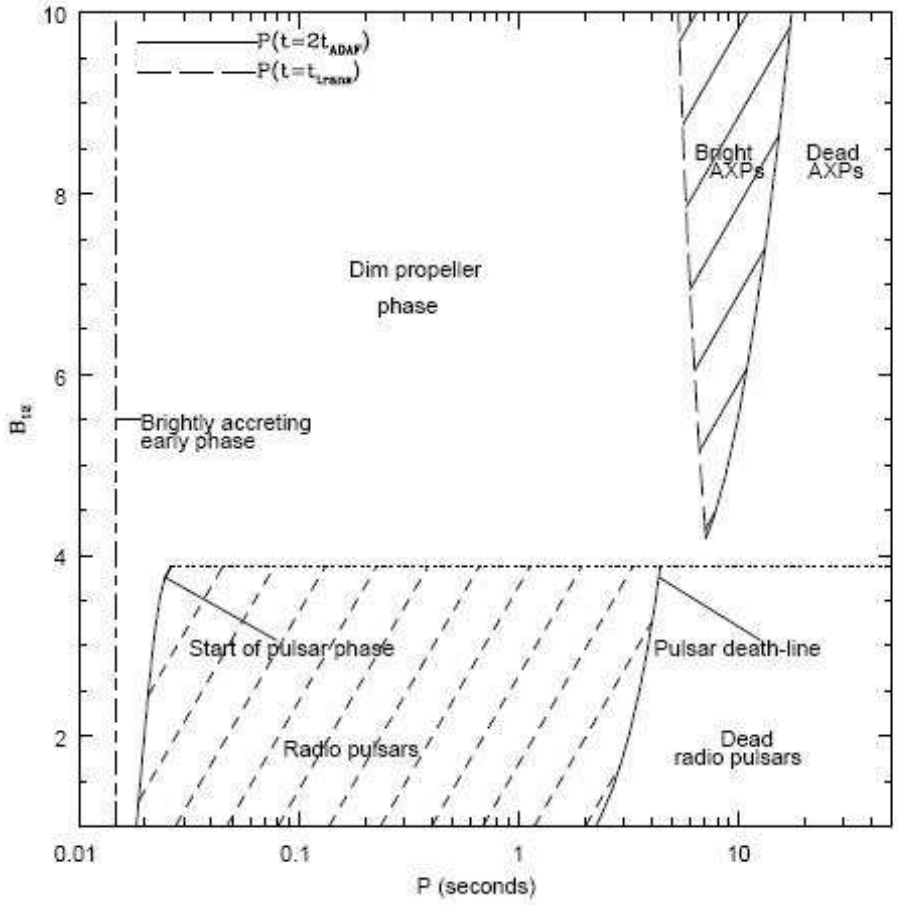

Figure 2.1: Phase evolution of a neutron star with an initial spin period of 0.015 s and accretion disk mass of 0.006 M_{sun} (Chatterjee et al. 2000).

CHAPTER 3

OBSERVATIONS

3.1 Observation History of SGRs and AXPs

Period and period derivatives are taken from the SGR/AXP Online Catalog compiled by McGill Pulsar Group. [1]

1. SGR 1900+14: This SGR was discovered in 1979 (Mazets et al. 1979). Between 1998 May and October, it emitted over 100 bursts and on 1998 August 27 a burst similar to the March 5 burst of the SGR 0526-66 was detected (Woods et al. 1999). Period of the SGR is $\sim$5.2 s and it has a period derivative of $\sim 7\times10^{-11}$ s/s (Woods et al. 2001).

2. SGR 0526-66: This SGR is the source of the 1979 March 5 burst (Mazets et al. 1979; Cline et al. 1980). It locates in the supernova remnant N49 of the Large Magellanic Cloud (Evans et al. 1980). Period of the source is $\sim$8 s. and period derivative is $\sim$6.5 $\times10^{-11}$ s/s. SGR 0526-66 currently acts like an AXP (Kulkarni et al. 2003).

3. SGR 1806-20: This SGR was discovered in January 1979 (Laros et al. 1987). Supernova relation of the object has not been confirmed yet. Object has a spin period of $\sim$7.6 s. and period derivative of $\sim$ 5.5 $\times10^{-10}$ s/s. Between

[1] McGill Pulsar Group, URL, http://www.physics.mcgill.ca/ pulsar/magnetar/main.html, August 2007

2004 September and October, 69 bursts with a detection of absorption feature at 4.2 keV and a giant flare with a peak luminosity of 2 $\times 10^{47}$ ergs s^{-1} on 2004 December 27 were observed (Mereghetti et al. 2005; Woods et al. 2007). Detailed spectral and timing history of 1806-20 between 1993 and 2005 can be found in the paper by Woods et al. 2007.

4. SGR 1627-41: This SGR was discovered in 1998 during its burst epoch (Woods et al. 1999) and within six weeks it emitted over 99 bursts with burst peak luminosities varying from 10^{39} to 10^{42} ergs s^{-1} (Woods et al. 1999). Period of the source is $\sim$6.4 s. Currently, period derivative of the source is not obtained. 1627-41 has also a supernova remnant (SNR) association. It locates in the supernova remnant G337.0-0.1.

5. AXP 4U 0142+61: This object has a period of $\sim$ 8.7 s and period derivative of $\sim 2\times 10^{-11}$ s/s. Optical pulsations were observed from this object (Kern & Martin, 2002) and Hulleman et al. (2004) found a sudden drop in flux between visible and blue band which is thought to be due to a spectral feature. Observation list is presented in Table 3.5.

6. AXP 1E 1048.15937: This AXP has a period of $\sim$ 6.4 s. and period derivative of $\sim 2.7\times 10^{-11}$ s/s, but spin-down rate of the object is not constant and shows significant deviations as compared to other two AXPs (1E 2259+586 and 1RXS J170849.0-400910) which time coherent timing was done. (Kaspi et al. 2001). On 2004 June 29 burst phenomena with significant spectral evolution was observed and this object is most likely the source of 2001 bursts which were detected in the direction of the object (Gavriil et al. 2006).

7. AXP 1E 2259+586: Period of the object is $\sim$ 7 s. and period derivative is $\sim 0.05\times 10^{-11}$ s/s. This AXP showed an outburst and a simultaneous glitch phenomena with significant spectral evolution in 2002 (Woods et al. 2004). Object locates in the SNR CTB 109.

8. AXP 1RXS J170849.0-400910: This object was discovered in 1996 (Sugizaki

et al., 1997). Period of the object is $\sim$ 11 s. and period derivative is $\sim 2 \times 10^{-11}$ s/s. Two glitches were detected in 1999 and 2001 with different recovery properties (Kaspi et al., 2000; Kaspi & Gavriil, 2003). 2001 glitch resembles to that seen in AXP 1E 2259+586 in 2002 (Kaspi & Gavriil, 2003).

9. AXP 1E 1841-045: Object is located in the SNR Kes 73. Period of the object is $\sim$12 s and period derivative is $\sim 4 \times 10^{-11}$ s/s.

10. AXP XTE J1810-197: This object was discovered in 2004 (Ibrahim et al. 2004). It is a transient AXP and showed burst phenomena (Woods et al. 2005). Period of the object is $\sim$ 5.5 s. and period derivative is $\sim 0.8 \times 10^{-11}$ s/s.

11. AXP CXOU J010043.1-721134: This object is in the Small Magellanic Cloud. Period of the object is $\sim$ 8 s. and spin-down rate is $\sim 2 \times 10^{-10}$ s/s. There is no evidence of variability was observed from this object over 25 years (McGarry et al. 2005).

12. AXP AX J1845-0258: This object is an unconfirmed AXP. Its location coincides with SNR G29.6+0.1 (Tam et al. 2007). Period of the object is $\sim$7 s. Currently, period derivative of the source is not obtained.

13. AXP CXO J164710.2-455216: This unconfirmed AXP was discovered in the Westerlund 1 which is a young and massive Galactic star cluster (Muno et al. 2006). Period of the object is $\sim$ 11 s. and period derivative is $\sim 2 \times 10^{-10}$ s/s.

Archival observations and obtained parameters of these objects are listed in Tables between 3.1-3.13 in order to see the spectral differences of these objects.

Marsden & White (2001) studied the spectral parameter variations with respect to the spin-down rate of AXPs and SGRs in their persistent states. They analyzed two SGR and five AXP data over the energy range 0.5-10.0 keV. Photon indices obtained from single power law fit were plotted with respect to the spin-down rate (Figure 3.1). Plots show that hardness of the spectra increases with increasing spin-down rate. They also fitted two component blackbody plus power law model which fits well to the AXP spectra to investigate the blackbody temperature, photon index and

L_{PL}/L_{BB} ratio variations with respect to the spin-down rate. Hardness of the spectra increases with respect to the spin-down rate for this model like the single component model but no variation in the temperature was found (Figure 3.2 and 3.3). Ratio of power law luminosity to blackbody luminosity show the same trend like hardness, increasing ratio with increasing spin-down rate (Figure 3.4).

They argued the models proposed to explain the AXP and SGR phenomena. X-ray binary membership of this objects was rejected because no correlation between the spectral parameters and the spin-down rate was found in X-ray binaries. L_{PL}/L_{BB} ratio proposed as a constraint for the magnetar model. Magnetar model predicts the L_{PL}/L_{BB} ratio decreases as a function of magnetic field and spin-down rate but in their analysis Marsden & White found a positive correlation. To obtain a decreasing ratio they proposed that the power-law emission must extend into the far-UV band.

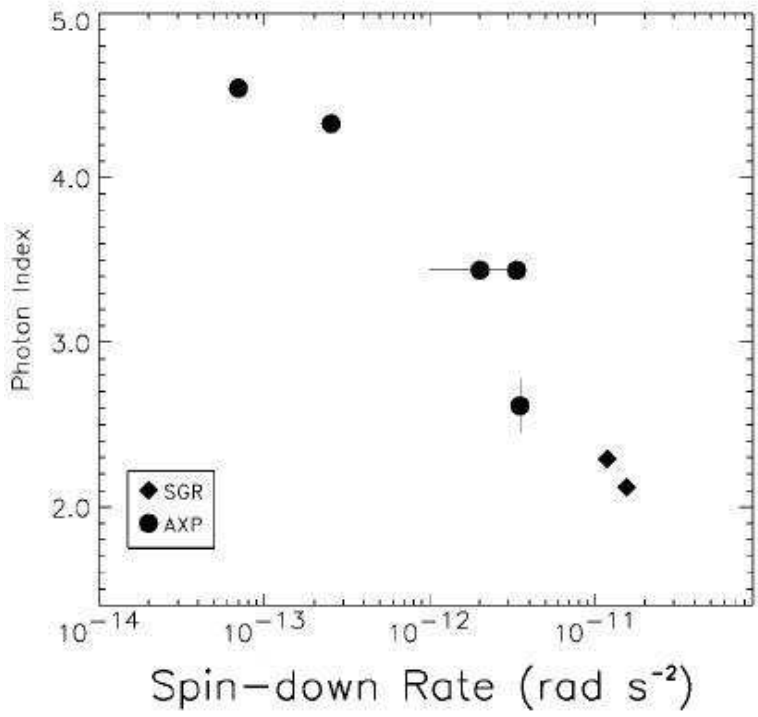

Figure 3.1: Variation of photon index with spin-down rate in single power law model (Marsden & White 2001).

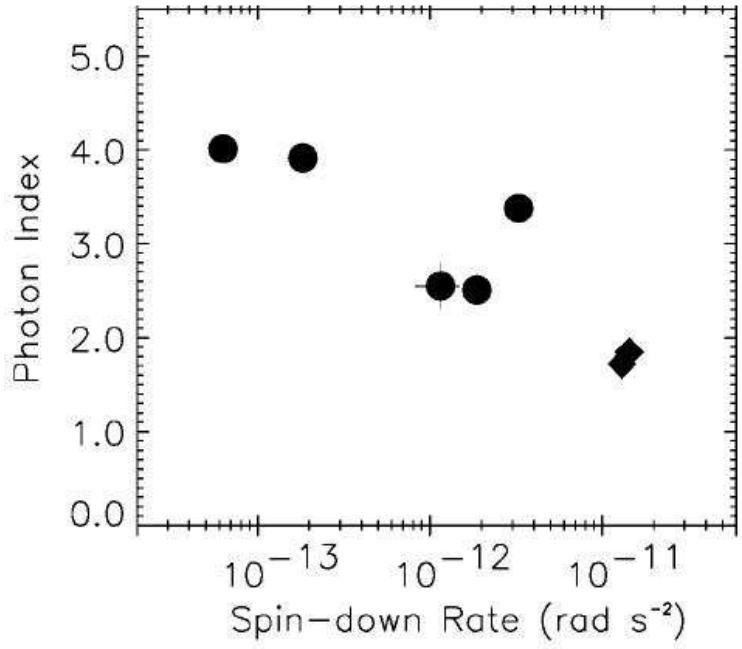

Figure 3.2: Variation of photon index with spin-down rate in two component blackbody plus power law model (Marsden & White 2001).

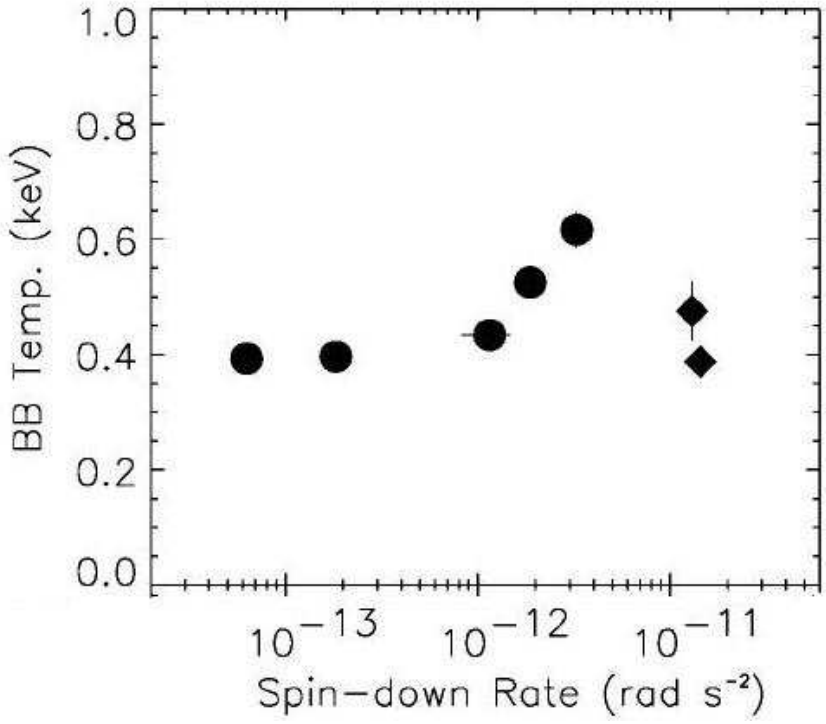

Figure 3.3: Variation of blackbody temperature with spin-down rate in two component blackbody plus power law model (Marsden & White 2001).

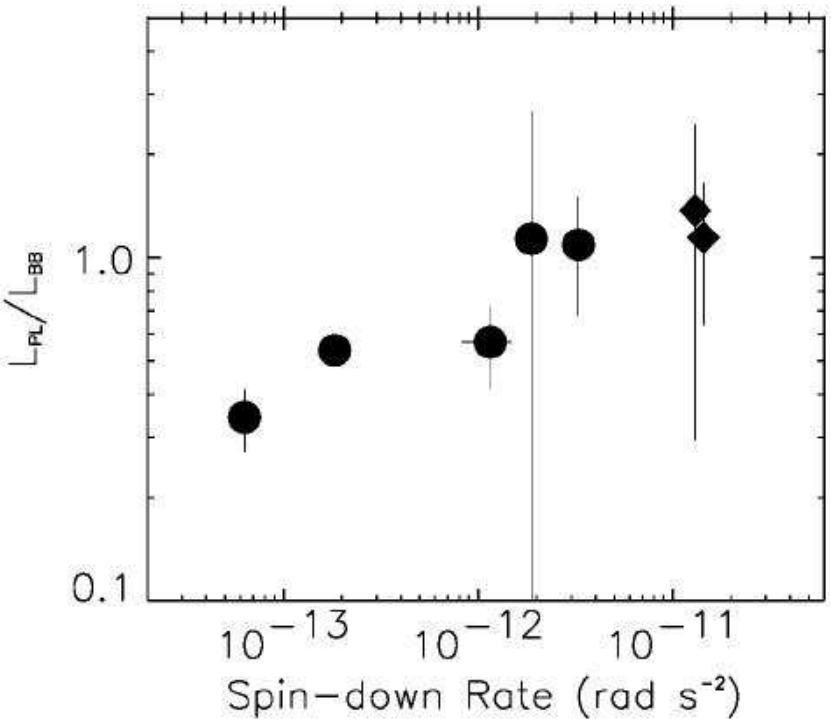

Figure 3.4: Variation of L_{PL}/L_{BB} ratio with spin-down rate in two component black-body plus power law model (Marsden & White 2001).

Table 3.1: Spectral Parameters of SGR 1900+14

Date	Satellite	Model	Power Law Index	NH 10^{22} cm^{-2}	BB Temp. or Gauss. (keV)	Unabsorbed Flux [a] 10^{-11} $\mathrm{erg\ cm^{-2}\ s^{-1}}$
May 1997	BeppoSAX[1]	BB+PL	1.1	1.8	0.51	0.99
April 1998	ASCA[2]	PL	2.25	2.16	-	0.96
June 1998	RXTE[3]	PL+Gaussian	2.1	3.4	6.6	4.4
August 1998	RXTE[3]	PL+Gaussian	3.1	5.5	6.5	9.9
September 1998[b]	BeppoSAX[1]	BB+PL	1.8	2.2	0.62	2.50
March,April 2000	BeppoSAX[1]	BB+PL	1.98	2.7	0.43	1.03
Setember 2005	XMM[4]	BB+PL	1.9	2.12	0.47	0.485
April 2006	XMM[4]	BB+PL	1.9	2.3	0.47	0.55
September 2005	XMM[4]	PL	2.84	2.57	–	0.48
April 2006	XMM[4]	PL	2.81	2.71	–	0.56

[a] Unabsorbed Flux 2.0-10.0 keV

[b] Active period

[1]Woods et al. 1999, 2001 [2] Hurley et al. 1999a [3] Kouveliotou et al. 1999 [3] Mereghetti et al. 2006

Table 3.2: Spectral Parameters of SGR 0526-66

Date	Satellite	Model	Power Law Index	NH 10^{22} cm^{-2}	Blackbody Temp. (keV)	Unabsorbed Flux [a] 10^{-12} $\mathrm{erg\ cm^{-2}\ s^{-1}}$
January 2000	Chandra[1]	BB+PL	3.1	0.54	0.6	3.52
August 2001	Chandra[1]	BB+PL	3.12	0.54	0.48	3.26

[a] Unabsorbed Flux 0.5-10 keV

[1] Kulkarni et al. 2003

Table 3.3: Spectral Parameters of SGR 1806-20

Date	Satellite	Model	Power Law Index	NH 10^{22} cm^{-2}	Bbody or Bremss Temp. (keV)	Unabs. Flux [a]	PL Flux[a]
Oct. 1993	ASCA[1]	PL	2.2	6.0	-	1.0	-
Oct. 98, Mar. 99	BeppoSAX[2]	PL	1.95	6.3	-	1.64	-
Oct. 98, Mar. 99	BeppoSAX[2]	Bremss.	-	5.35	11.0	1.50	-
Apr. 2003	XMM[3]	BB+PL	1.44	6.64	0.59	-	1.16
July 2003	CHANDRA[6]	BB+PL	1.57	8.0	0.48	2.20	-
July 2003	CHANDRA[6]	PL	1.89	7.1	-	1.95	-
Oct. 2003	XMM[3]	BB+PL	1.2	6.05	0.73	-	1.25
June 2004	CHANDRA[6]	BB+PL	1.47	8.5	0.49	3.76	-
June 2004	CHANDRA[6]	PL	1.77	7.7	-	3.38	-
Sep. 2004[b]	XMM[3]	BB+PL	1.21	6.51	0.79	–	2.42
Oct. 2004[b]	XMM[3]	BB+PL	1.23	6.53	0.77	–	2.41
Apr. 2003	XMM[3]	PL	1.63	6.31	–	–	1.226
Oct. 2003	XMM[3]	PL	1.55	6.10	–	–	1.379
Sep. 2004[b]	XMM[3]	PL	1.51	6.69	–	–	2.651
Oct. 2004[b]	XMM[3]	PL	1.57	6.70	–	–	2.670
Mar. 2005	XMM[4]	BB+PL	0.8	6.0	0.91	–	1.92
Feb. 2005	CHANDRA[5]	PL	1.8	7.1	–	-	-
Feb. 2005	CHANDRA[5]	BB+PL	1.78	7.5	<0.93	-	-
Oct. 2005	XMM[6]	BB+PL	1.19	6.6	0.77	2.0	-
Oct. 2005	XMM[6]	PL	1.83	7.2	-	2.08	-

[a] $\times 10^{-11} \mathrm{erg\ cm^{-2}\ s^{-1}}$ over $2-10$ keV

[b] Active phase

[1] Sonebe et al. 1994 [2] Mereghetti et al. 2000 [3] Mereghetti et al. 2005

[4] Tiengo et al. 2005 [5] Rea et al. 2005 [6] Woods et al. 2007

Table 3.4: Spectral Parameters of SGR 1627-41

Date	Satellite	Model	Power Law Index	NH 10^{22} cm^{-2}	Unabsorbed Flux [a] 10^{-12} $\mathrm{erg\ cm^{-2}\ s^{-1}}$
August 1998	BeppoSAX[1]	PL	2.6	10	5.9
September 1998	BeppoSAX[1]	PL	2.8	10	4.6
August 1999	BeppoSAX[1]	PL	1.9	5	1.1
February 1999	ASCA[2]	PL	3.24	9[b]	2.76
September 2000	BeppoSAX[1]	PL	3.0	8	1.1
September 2001	Chandra[2]	PL	2.17	9[b]	0.267
August 2002	Chandra[2]	PL	2.95	9[b]	0.266
February 2004	XMM[1]	PL	3.2[b]	9[b]	0.32
September 2004,4	XMM[1]	PL	3.2[b]	9[b]	0.26
September 2004,22	XMM[1]	PL	3.2	9[b]	0.23
September 2004,22	XMM[1]	PL	3.7	11.4	0.32

[a] Unabsorbed Flux over 2.0–10.0 keV

[b] Fixed Value

[1] Mereghetti et al. 2006 astro-ph/0512059v2 [2] Kouveliotou et al. 2003

Table 3.5: Spectral Parameters of AXP 4U 0142+61

Date	Satellite	Model	Power Law Index	NH 10^{22} cm^{-2}	Blackbody Temp. (keV)	Bremss. (keV)	Absorbed Flux [a] 10^{-11} $\mathrm{erg\ cm^{-2}\ s^{-1}}$
1994 Sep.	ASCA[1]	BB+PL	3.67	0.95	0.386	-	13[a]
1994 Sep.	ASCA[1]	BB+Brems.	1.56	0.9	-	0.93	13[a]
1997 Jan.	BeppoSAX[2]	BB+PL	3.8	1.1	0.37	-	-
1998 Feb.	BeppoSAX[2]	BB+PL	4.0	1.2	0.41	-	-
1998 Aug.	ASCA[3]	BB+PL	3.3	0.97	0.384	-	13.4[b]
1998 Sep.	ASCA[3]	BB+PL	3.3	0.92	0.380	-	13[b]
2000 May	Chandra[4]	BB+PL	3.35	0.91	0.458	-	-
2001 May	Chandra[5]	BB+PL	3.3	0.88	0.418	-	-
2001 May	Chandra[5]	BB+Brems.	-	0.69	-	1.6	-
2001 May	Chandra[5]	Brems.	-	0.92	-	1.11	-
2001 May	Chandra[5]	CutOffPL	0.9	0.83	-	-	-

Note: E_{cut} for PL=0.93 keV

[a] 0.5-10.0 keV

[b] 2.0-10.0 keV

[1] White et al. 1996 [2] Israel et al. 1999 [3] Paul et al. 2000 [4]Patel et al. 2003 [5]Juett et al. 2001

Table 3.6: Spectral Parameters of AXP 1E 1048.1-5937

Date	Satellite	Model	Power Law Index	NH 10^{22} cm^{-2}	Bbody Temp. (keV)	Unabsorbed Flux [a] 10^{-12} $\mathrm{erg\ cm^{-2}\ s^{-1}}$
1994 March	ASCA[1]	BB+PL	2.9	1.0	0.57	5.8
1997 May[b]	BeppoSAX[2]	BB+PL	3.3	1.2	0.62	7.1
1998 July	ASCA[1]	BB+PL	3.2	1.21	0.56	6.0
2000 December	XMM[3]	BB+PL	2.9	0.96	0.63	-
2002 August	Chandra[3]	BB+PL	2.7	1.11[c]	0.62	-
2003 June	XMM[4]	BB+PL.	3.27	1.08	0.627	-
2004 July	XMM[4]	BB+PL	3.44	1.10	0.623	-
2004 July	CHANDRA[5]	BB+PL	3.30	1.18	0.619	
2004 July	CHANDRA[5]	BB+PL	3.08	1.18	0.585	9.56
2004 July	CHANDRA[5]	BB+PL	3.23	1.23	0.585	9.2

[a] If not mentioned all Unabsorbed Fluxes are in the 2.0-10.0 keV band

[b] Reanalysis of the observation reported by Oosterbroek et al. 1998

[c] Fixed value

[1] Paul et al. 2000 [2] Tiengo et al. 2002 [3] Mereghetti et al. 2004 [4] Tiengo et al. 2005

[5] Gavriil et al. 2006

Table 3.7: Spectral Parameters of AXP 1E 2259+586

Date	Satellite	Model	Power Law Index	NH 10^{22} (cm^{-2})	Bbody Temp. (keV)	Unabsorbed Flux [a] $(10^{-11}$ erg cm^{-2} $\mathrm{s}^{-1})$
1990 December	BBXRT[1]	PL	3.86	1.01	-	
1990 December	BBXRT[1]	BB+PL	3.34	0.88	0.329	-
1993 May	ASCA(S0)[1]	BB+PL	3.04	0.67	0.415	-
1993 May	ASCA(G2)[1]	BB+PL	3.15	0.43	0.418	-
1993 May	ASCA(G3)[1]	BB+PL	3.29	0.48	0.423	-
1996 November	BeppoSAX[2]	BB+PL	3.93	0.87	0.44	-
2000 January	CHANDRA[3]	BB+PL	3.6	0.93	0.412	2.0
2002 January[b]	XMM[4]	BB+PL	4.04	1.096	0.488	1.53
2002 June 6[b]	XMM[4]	BB+PL	4.10	1.098	0.411	1.63
2002 June 21[c]	XMM[4]	BB+PL	3.59	1.035	0.517	4.17
2002 July 9[c]	XMM[4]	BB+PL	3.62	0.953	0.537	2.37
2002 July 9[c]	XMM[4]	BB+PL	3.58	0.937	0.548	2.49

[a] If not mentioned all Unabsorbed Fluxes are in the 2.0-10.0 keV band

[b] Before burst

[c] After burst

[1] Corbet et al. 1995 [2] Parmar et al. 1998 [4] Patel et al. 2001 [3] Woods et al. 2004

Table 3.8: Spectral Parameters of AXP 1RXS J170849-400910

Date	Satellite	Model	Power Law Index	NH 10^{22} cm^{-2}	Bbody Temp. (keV)	Unabs. Flux[a]
1999 March	BeppoSAX[1]	PL	3.28	1.88	-	-
1999 March	BeppoSAX[1]	BB+PL	2.62	1.42	0.46	-
1999 March	BeppoSAX[1]	BB+BB	-	0.9	0.50-1.54	-
2003 August	XMM[2]	BB+PL	2.83	1.48	0.456	9.1
2004 July	CHANDRA[3]	BB+PL	2.74	1.36	0.42	13

[a] Unabsorbed Fluxes are in the 0.5-10.0 keV band [a] 10^{-11} $\mathrm{erg\ cm^{-2}\ s^{-1}}$

[1] Israel et al. 2001 [2] Oosterbroek et al. 2004 [3] Campana et al. 2007

Table 3.9: Spectral Parameters of AXP 1E 1841-045

Date	Satellite	Model	Power Law Index	NH 10^{22} cm^{-2}	Bbody Temp. (keV)	Unbsorbed Flux [a] 10^{-11} $\mathrm{erg\ cm^{-2}\ s^{-1}}$
1998 March	ASCA[1]	PL	3.38	2.21	-	
1999 March/April	ASCA[1]	PL	3.46	2.26	-	
2000 July	Chandra[2]	BB+PL	2.0	2.54	0.44	5.0
2000 July	Chandra[2]	BB+BB	–	2.34	0.47/1.5	4.1

[a] Unabsorbed Fluxes are in the 0.6-7.0 keV band

[1] Mereghetti et al. 2002 [2] Morii et al. 2003

Table 3.10: Spectral Parameters of AXP XTE J1810-197

Date	Satellite	Model	Power Law Index	NH 10^{22} cm^{-2}	Bbody Temp. (keV)	Absorbed Flux [a] 10^{-11} $\mathrm{erg\ cm^{-2}\ s^{-1}}$
2003 September[b]	XMM[1]	BB+BB	-	0.65	0.26/0.68	3.93
2003 September[b]	XMM[1]	BB+PL	3.7	1.05	0.67	3.98
2003 October[b]	XMM[1]	BB+BB	-	0.65	0.29/0.71	3.84
2004 March	XMM[1]	BB+PL	3.75	1.02	0.68	2.16
2004 March	XMM[1]	BB+BB	-	0.65	0.27/0.70	2.13
2004 September	XMM[1]	BB+BB	-	0.65	0.25/0.67	1.29
2005 March	XMM[1]	BB+BB	-	0.65	0.22/0.60	0.567
2005 September	XMM[1]	BB+BB	-	0.65	0.20/0.52	0.235
2006 March	XMM[1]	BB+BB	-	0.65	0.19/0.46	0.144

[a] Fluxes are in the 0.5-10.0 keV band.

[b] 2003 observations were obtained in the high state of the pulsar.

[1] Gotthelf&Halpern 2004, 2005, 2006 Gotthelf et al. 2004

Table 3.11: Spectral Parameters of AXP CXOU J010043.1-721134

Date	Satellite	Model	Power Law Index	NH[a] 10^{22} cm^{-2}	Bbody Temp. (keV)	Unbsorbed Flux [b] 10^{-13} $\mathrm{erg\ cm^{-2}\ s^{-1}}$
2000 October	XMM[1]	BB+PL	1.8	0.1	0.35	5
2001 May	CHANDRA[1]	BB+PL	1.9	0.8	0.36	5
2001 November	XMM[1]	BB+PL	2.0	0.6	0.3	5
2004 January	CHANDRA[1]	BB+PL	2.0	0.3	0.38	4
2004 February	CHANDRA[1]	BB+PL	2.0	0.3	0.38	4
2004 March	CHANDRA[1]	BB+PL	2.0	0.3	0.38	4

[a] Absorbing column due to the Small Magellanic Cloud only.

[b] Unabsorbed Fluxes are in the 0.5-10.0 keV band

[1] McGarry et al. 2005

Table 3.12: Spectral Parameters of AXP candidate AX J1845-0258

Date	Satellite	Model	Power Law Index	NH 10^{22} cm^{-2}	Bbody Temp. (keV)	Absorbed PL or BB Flux [a] 10^{-13}
June-September 2003	CHANDRA[1]	BB	-	5.6	2.0	2.6
June-September 2003	CHANDRA[1]	PL	1.0	7.8	-	2.8

[a] Fluxes are in the 2.0-10.0 keV band ($\mathrm{erg\ cm^{-2}\ s^{-1}}$)

[1] Tam et al. 2006

Table 3.13: Spectral Parameters of AXP candidate CXO J164710.2455216

Date	Satellite	Model	Power Law Index	NH[a] 10^{22} cm^{-2}	Bbody Temp. (keV)	Absorbed Flux [b] 10^{-13} $\mathrm{erg\ cm^{-2}\ s^{-1}}$
2005 May&June	CHANDRA[1]	BB	-	1.2	0.61	2.4

[a] Absorbing column due to the Small Magellanic Cloud only. [b]

Unabsorbed Fluxes are in the 0.5-8.0 keV band

[1] Tam et al. 2006

CHAPTER 4

INSTRUMENTS

Information about XMM-Newton is compiled from XMM Users' Handbook, Issue 2.4.[1], about RXTE from the XTE Technical Appendix, Appendix F[2], and about Chandra, The Chandra Proposers' Observatory Guide version 9.0 [3].

4.1 X-ray Multi Mirror Mission

XMM-Newton was launched on 10 December 1999 by Ariane-5 with an orbital period of 48 hours and inclination of 40 degrees to observe X-rays which are obstructed by Earth's atmosphere. Satellite takes its name from the Multi-Mirror design and Isaac Newton for his pioneering contributions to the spectroscopy. Owing to its highly eccentric orbit, long observations can be done without interruption up to about 40 hours, and 5 main cameras can be cooled to between $-80^{\circ}\mathrm{C}$ to $-100^{\circ}\mathrm{C}$ easily (Jansen et al. 2001). Investigation of spectra of cosmic X-ray sources with X-ray fluxes as low as $10^{-15}\ \mathrm{erg\ cm^{-2}s^{-1}}$ (Jansen et al. 2001), acquiring sensitive medium-resolution spectroscopy with resolving powers between 100 and 700 over the wavelength band 350 - 2500 eV, broad-band imaging spectroscopy from 100 eV to 15 keV, multi wavelength studies between 1600 - 6000 Å with a designated optical

[1]XMM Newton Science Operations Centre, URL, http://xmm.vilspa.esa.es/external/xmmusersupport/documentation/uhb/XMMUHB.html, June 2007

[2]NASA, ftp://legacy.gsfc.nasa.gov/xte/nra/appendix-f/, June 2007

[3]Chandra X-ray Observatory, URL, http://cxc.harvard.edu/proposer/POG/pdf/MPOG.pdf, June 2007

monitor are the main objectives of the mission (ESA SP-1268 2003). XMM-Newton has three Wolter-Type X-ray telescopes. To maximize the effective area, the mirrors of each X-ray telescopes are made of 58 nested Wolter-1 grazing incidence optics which has a focal length of 7.5 m, grazing incidence angles between 17 and 42 arcmin. Geometric effective area of telescopes is 1550 cm^2 for each telescope at 1.5 kev and 4650 cm^2 in total.

10 meters length satellite contains three main instruments on board:

1. European Photon Imaging Cameras (EPIC)

2. Reflection Grating Spectrometers (RGS)

3. The Optical Monitor (OM)

EPIC consists of three CCD operating on the focal plane of Wolter-Type X-ray telescopes for X-ray imaging, medium-resolution spectroscopy and photometry. Two of three are called EPIC-MOS (Metal Oxide Semiconductor) and the other EPIC-PN which has a different design. EPIC-MOS has seven CCDs with pixel sizes 40 μm and EPIC-PN contains 12 CCDs with 150 μm. Cameras are capable of measuring the arrival time, impact position on the detector and the energy of X-ray photons.

RGS consists of two spectrometers which enable high-resolution spectroscopy. These are also on the focal plane of Wolter-Type X-ray telescopes like EPIC cameras.

Optical Monitor is mounted on a separate telescope and designed for optical/UV imaging and grism spectroscopy, enabling detection of optical counterparts of X-ray sources. All of these instruments can operate simultaneously. See Figure 4.1 for the design and instruments.

4.1.1 Data Acquisition Modes

Full-Frame and Extended-Full Frame Mode : Only the PN camera can operate in these modes. All pixels of all CCDs are read out. Extended means image collection time, frame time, is longer than the full frame mode (Figure 4.2).

Partial Window Mode : In this mode only a part of the CCDs is read out. For MOS only central CCD can be operated in this mode. For PN in small window mode only CCD number 4 is operated but in the large window mode half of the area of CCDs is read out (Figure 4.2).

Timing Mode : To increase speed of reading, data is collapsed into one dimensional-row. For only PN camera there is another mode called Burst Mode with very high time resolution. But in this mode source position is not read out contrary to timing mode.

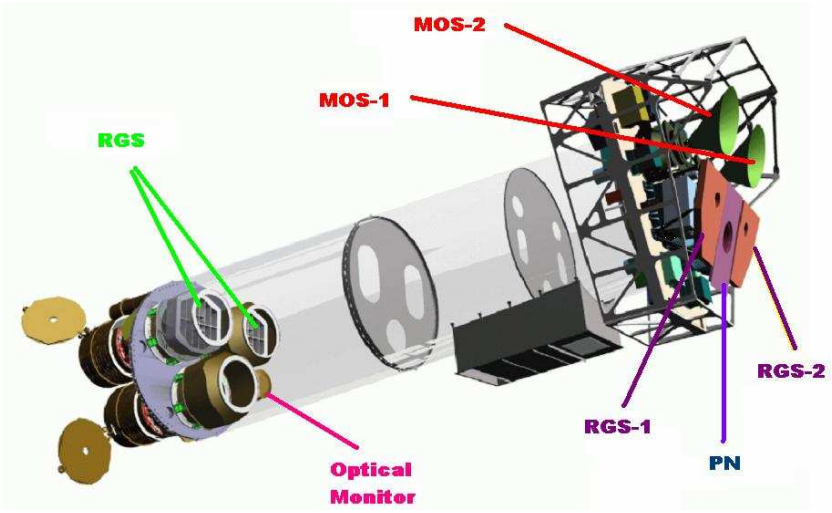

Figure 4.1: XMM-Newton Instruments

4.1.2 European Photon Imaging Camera

EPIC-MOS and PN cameras are designed for sensitive imaging observations in the energy range of 0.15 to 15.0 keV with spectral resolution 20 - 50 and angular resolution 6 arcsec at Full Width Half Maximum (FWHM). Field of view (FOV) of cameras is 30 arcmin and they can operate in different modes with different time resolution.

During the analysis, astrophysicist may encounter with some problems because of the electronics of detectors, cosmic ray particles etc. So, handicaps of the instru-

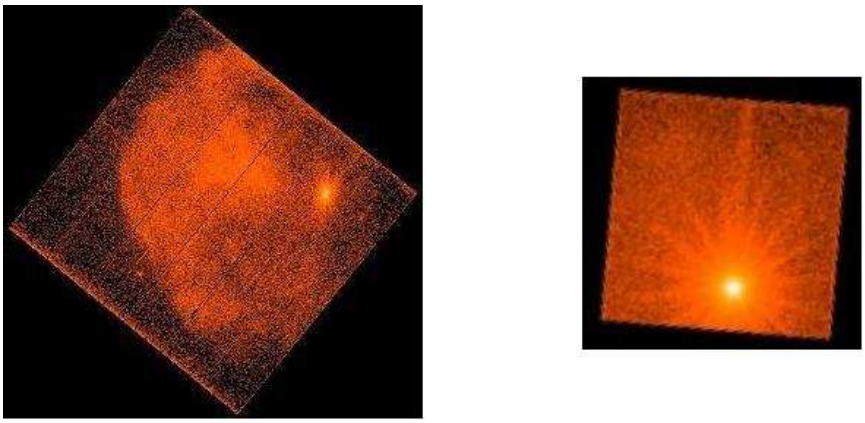

Figure 4.2: EPIC-PN Extended Full-frame and Small-Window Mode. The object is 1E 2259+586

ments must be well known. Some problems are presented below. But for further details we recommend you to read Users' Guide.

Interaction of particles with detector environment (dominant above a few keV), detector noise (dominant at low energies i.e below 200 eV), soft proton flares and, strong metal line features generate the EPIC background. Soft proton flares with proton energies less than a few 100 keV can affect the detectors significantly and are generated by the funneling of protons to the detector via X-ray mirrors. Also their identification due to the correlation between spectral shape and intensity is impossible. At the beginning of analysis a high energy light curve should be created to specify the intervals of flaring particle background. MOS spectrum shows Al-Kα and Si-Kα due to the fluorescence at 1.5 and 1.7 keV respectively, and PN spectrum shows inhomogeneous Al-Kα, Cu- Kα, Ni- Kα, Z- Kα lines around 8 keV. The intensity due to this components are 2.2 x 10^{-3} cts cm^{-2} s^{-1} keV^{-1} for MOS and 5 x 10^{-3} cts cm^{-2} s^{-1} keV^{-1} for PN camera. Also there is a rise below 0.5 keV in the background spectrum because of the detector noise of both cameras.

Pile-up is an important effect that occurs when two or more photons arrive to a pixel or an adjacent pixel before the read out process. This causes the loss of flux because of the artificial hole in the center of Point Spread Function (defines the focusing ability of a mirror) via the photons coming at the same time. Also combination of a

few soft photons can generate hard photons which affects the spectral response's of detectors and causes energy distortion. So, if count rate is above the pile-up limit it can be important especially for extended sources. For point-like sources good results can be obtained even if the pile-up is above the limit. SAS command 'epatplot' is used to see whether source is affected by pile-up or not.

In the imaging mode if photons arrive to detector at the time of read-out Out-of-Time events occur due to the shifting of charges during the read-out which confuses the frame of events. This effect broadens the spectral features. To overcome this effect, firstly an OoT event file should be created by using SAS task 'epchain', then with this file an image or spectrum should be created in order to subtract them from the original image and spectra.

4.2 Rossi X-ray Timing Explorer

Satellite was launched on December 30, 1995 by Delta II rocket with an orbital period of 90 min. and inclination of 23 degrees. RXTE is important especially because of its fine timing resolution. It is convenient to study fast X-ray variability with RXTE in the energy range 2-250 keV. Data can be stored during 4 orbits without transmitting (Glasser et al. 1994).

There are three instruments on board:

1. Proportional Counter Array (PCA)
2. The High Energy X-ray Timing Experiment (HEXTE)
3. All Sky Monitor (ASM)

PCA and HEXTE are co-aligned instruments operating in different energy ranges. HEXTE operates between 15-250 keV with energy resolution 18% at 60 keV and has an effective area of 1200 cm^2 at 50 keV. Time resolution of HEXTE is 10 μs. ASM observes 80% of the sky every 90 minutes in the energy range 2-10 keV and can response the transient phenomena rapidly. Satellite has a maneuver capability of 180

degrees in less than 30 minutes. So, within a few hours phenomena can be observed by PCA or HEXTE. See Figure 4.3 for the design and instruments.

There are some constraints on the observation time and viewing area of RXTE. For example, RXTE should not be closer than 30 degrees to the Sun. Also it suffers from the South Atlantic Anomaly (SAA) because of its low-Earth equatorial orbit and low geomagnetic rigidity regions where the high energy background is enhanced. Earth occultation is another constraint on the observation time and it can interrupt the observation generally through 30 minutes.

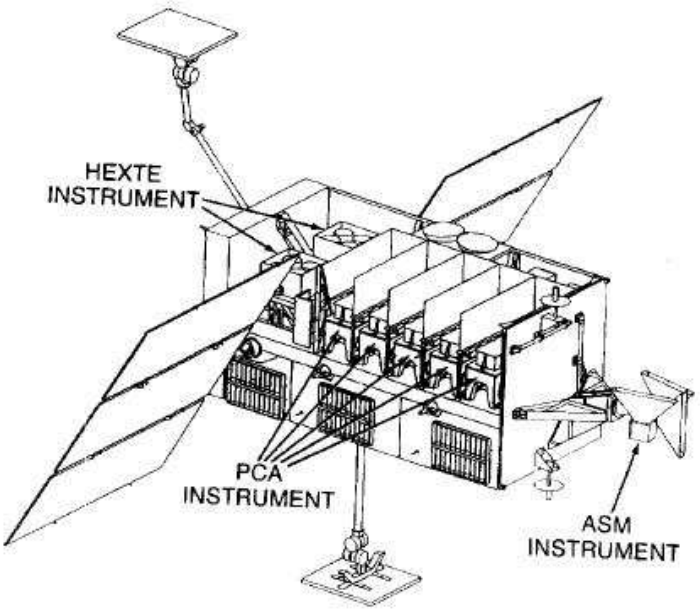

Figure 4.3: RXTE Instruments. Picture is taken from Glasser et al., 1994

4.2.1 Proportional Counter Array

Principle physical mechanism of proportional counters is photoelectric absorption under 50 keV. When a high energy particle passes from a proportional counter it interacts with the molecules of gas which fills the detector. Then, an electron-ion pair forms. If the frequency of the photon is ν then, the energy of the photon is E=hν.

When this photon interacts with the molecules of the gas it can eject electrons with binding energies equal to or smaller than hν. The difference between the binding energy of the electron and energy of the photon is transferred to the electron as a kinetic energy. Then, electrons drift to the anode and ions drift towards the cathode under the influence of external electric field. During the motion of electrons and collision with the molecules of gas they are accelerated by the external field and reach energies higher then the thermal value in contrast with ions. So, electrons acquire sufficient energy to produce new electron-ion pairs. On the other hand, ions deexcite by emitting a fluorescent X-ray or an Auger electron which is a secondary electon ejected after the emission of an electron from atom. As a result electrons induce a signal when they reach the anode. The strength of the signal is proportional to the amount of ionization produced by particles and photons. This is the reason why these detectors are called proportional counters. The energy sensitivity of the detector is determined by the absorption cross-section of the gas (Longair 1992).

RXTE's PCA consists of 5 identical collimated Proportional Counter Units (PCU), numbered from 0 to 4, operating in the energy range 2-60 keV with energy resolution 18% at 6 keV and each have an effective area of 1400 cm^2. Detecting volume is filled with 90% Xenon and 10% Methane gas (Glasser et al. 1994). PCA has a FOV of 1° at FWHM and time resolution of 1 μs. PCUs have two volumes such that one is filled with propane and the other with xenon/methane. The propane volume has a single layer of anodes while the xenon/methane volume has four layers of anode. The nominal operating thermal range of the PCUs is $-10^\circ\mathrm{C}$ to $+25^\circ\mathrm{C}$.

Data acquisition modes and formating are controlled by Experiment Data System (EDS) for the PCA and ASM to remove the strain on telemetry resources. There are 7 and 3 modes for PCA and ASM respectively.

4.2.2 Data Modes for PCA

In our analysis we have used binned data and event encoded data modes. There are also five different data mode for PCA. These are single bit code mode, burst catcher mode, delta binned mode, fast fourier transform mode and pulsar-fold mode.

Data is processed by the on board EDS. EDS has six 'Event Analyzers' (EA) which are used by PCA. Selection, rejection and processing of detected events are done by EDS. EDS runs 7 modes for the PCA depending on the parameters like energy bin boundaries, time bin widths and type of event. Two of the EAs run in the Standard-1 and Standard-2 configurations. The others are selected by the observers.

The output of the 'Binned Data Mode' is time-binned histograms. Time bin duration is selectable between the interval of 0.954 μs - 4096 s. Standard-1 and 2 are the configurations runned in this mode.

Standard-1: Time resolution of this mode is 0.125 seconds. All 256 channels are combined into one channel, thus there is no energy resolution.

Standard-2: Time resolution is 16 seconds. This configuration has 129 channels.

'Events Encoded' mode is suitable for the rapid timing of faint sources. This mode yields data as time series. Good Xenon configuration of this mode uses two EAs and produce spectral and temporal information with a time resolution of ~ 1 μs and it has 256 channels.

4.3 Chandra X-ray Observatory

Chandra X-ray Observatory was launched on July 23, 1999. It completes its elliptical orbit in 63.5 hours and observations up to 55 hours can be done without interruption. Optics of the telescope consist of Wolter Type-I grazing incidence X-ray mirrors like XMM-Newton with an effective area of 400 cm^2 at 5 keV and focal length of 10.066 m. Satellite is above the radiation belts about the 75 $\%$ of its orbital time. See Figure 4.4 for design and instruments.

Science Instruments:

1. Advanced CCD Imaging Spectrometer (ACIS)
2. High Resolution Camera (HRC)
3. High Energy Transmission Grating (HETG)
4. Low Energy Transmission Grating (LETG)

ACIS and HRC are the focal plane instruments. HRC consists of two microchan-

nel plate detectors formed by the array of several electron multipliers which work with basic physical undergrounds such as photoelectric effect and acceleration voltage. One of the detectors is for wide-field imaging (HRC-I) in the energy range of 0.1 - 10 keV and its FOV is 30 arcmin x 30 arcmin. The other is for grating spectra (HRC-S) which works in the energy range of 0.08 - 6 keV and its FOV is 6 arcmin x 99 arcmin.

HETG is capable of obtaining high resolution X-ray spectra with a resolving power up to 1000 over the range 0.4 - 8.0 keV. It consists of two gratings called Medium Energy Grating (MEG) which covers an energy range of 0.4-5.0 keV, and High Energy Grating (HEG) with energy range of 0.8-10.0 keV. Effective area of the HETG is 7 cm^2 at 0.5 keV. Energy resolution for HEG is 0.012 Å and for MEG is 0.023 Å at FWHM.

LETG and HETG have similar design but LETG is modified for the energies up to 1 keV. LETG operates mainly with HRC-S and with also ACIS-S. LETG Spectrometer provides high resolution spectroscopy, resolving power up to 1000 ($E/\Delta E$) over the energy range of 0.07-0.15 keV and energy resolution of 0.05 Å at FWHM which provides the studies of spectral line profiles.

ACIS consists of two CCD array with an effective area of 600 cm^2 at 1.5 keV. ACIS-S has 6 CCD (1024 x 1024 pixel) for imaging, spectrometry and high resolution spectroscopy via the cooperation with HETG and LETG. ACIS-I has 4 CCD (1024 x 1024 pixel) for imaging and spectrometry.

ACIS has two operating mode:

1. Timed Exposure Mode (TE)

In this mode data is collected within a specified span called frame time between 0.2 to 10.0 seconds, and transfer occurs at the end of this specified time. Frame time is 3.2 seconds when all of the CCDs operate. If the frame time is shorter than the nominal time, 3.2 s., then, there will be dead times with no data is taken. Frame time bigger than 3.2 s increases the pile-up probability. Also nominal time can be changed by selecting a region of CCD which is called subarrays rather than full frame. Then, nominal time depends on the number of rows between subarray and

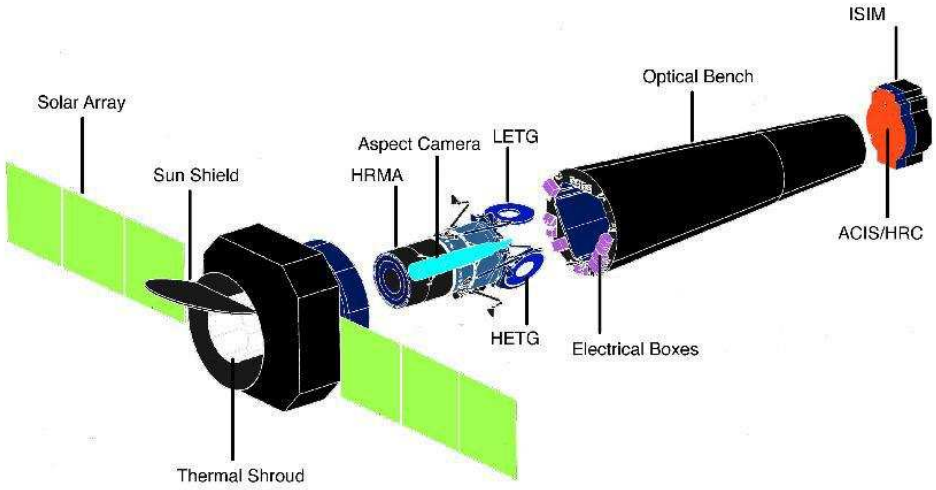

Figure 4.4: Chandra Instruments.

framestore region, the number of rows in the subarray, and total number of activated CCDs. Selection of a frame time less or more than the nominal time results in the effects as in the full frame.

2. Continuous Clocking Mode (CC)

CC mode obtains 1 pixel x 1024 pixel images each with an integration time of 2.85 msec which enables high time resolution but causes the loss of spatial resolution. Time is recorded as read-out time in continuous clocking mode which needs to be converted to the time of arrival with the CIAO tool acis_process_events.

CHAPTER 5

ANALYSIS AND RESULTS

5.1 AXP 1E 2259+586

Fahlman & Gregory announced the discovery of 1E 2259+586 with a period of about 7 second within the supernova remnant G109.1-1.0 in 1981 with the first X-ray imaging telescope of NASA, Einstein X-ray Observatory. SNR has a semicircular shape at both X-ray and radio wavelengths. Interaction of SNR with a molecular cloud is believed to be the reason of the shape (Tatematsu et al. 1987) (Figure 5.1). Distance of 3.0 $\pm$ 0.5 kpc and age of (8.8 $\pm$ 0.9) x $10^3 d_3$ yr. (d_3=(distance)/(3.0 kpc)) was estimated for the supernova remnant (Kothes et al. 2002; Sasaki et al. 2004).

1E 2259+586 has showed an outburst including 80 X-ray bursts with an accompanying glitch, changes in the X-ray properties on June 18, 2002 (Woods et al. 2004) and a near-infrared flux enhancement (Kaspi et al. 2003). Later, Tam et al. (2004) showed the association of infrared (IR) enhancement and outburst, and also showed the correlation of postoutburst IR and X-ray radiation. The IR variability has been detected from the AXPs 1E 1048.1-5937 and 4U 0142+61 but absence of X-ray flux variability has led people to think the correlated variation arises from an outburst after the detection of such variability in the transient AXP XTE J1810-197 (Rea et al. 2004).

Iwasawa et al. (1992) published the spin-down history with a secular spin-down trend for more than 10 years. But between 1987 and 1990 they reported a decrease in the spin-down rate with an increase in X-ray flux. Also, Baykal & Swank (1996)

have reported a spin-up episode during the ROSAT observations between 1991 and 1992, and Woods et al. (2004) published the spin rate change which precedes the outburst.

In this chapter we present the analysis of RXTE PCA, Chandra ACIS and XMM-Newton EPIC PN observations of AXP 1E 2259+586 in order to investigate long-term spin-down rate and spectral variabilities. All data processed in this chapter were acquired from NASA's HEASARC archive[1].

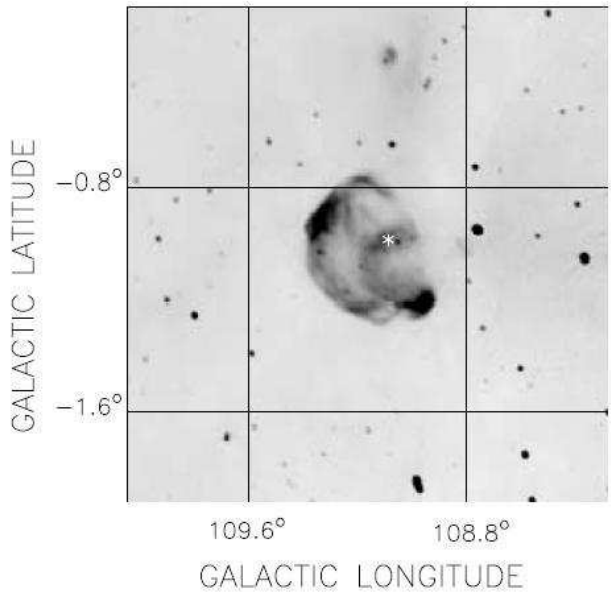

Figure 5.1: Supernova Remnant CTB 109. Radio continuum image of Supernova Remnant CTB 109 at 1420 MHz taken from the Canadian Galactic Plane Survey. Asterix shows the position of AXP 1E 2259+586 (Kothes et al. 2002)

[1]NASA's High Energy Astrophysics Science Archive Research Center (HEASARC), URL, http://heasarc.nasa.gov/docs/archive.html, July 2007

5.2 Chandra Analysis of 1E 2259+586

Chandra observed 1E 2259+586 on 2000 January 11. Data were obtained in CC and TE mode by using the Advanced CCD imaging spectrometer with 12 ks exposure time. Data were processed with using standard Chandra Interactive Analysis of Observations (CIAO). Source and background were extracted from CC mode as discussed in Patel et al. (2001). The feature between 1.9-2.1 keV appears in the spectrum is due to the iridium-edge structure in the telescope response. We ignored this region and fitted data with blackbody plus power law modified by interstellar absorption by using XSPEC version 12.3.1. The best fit parameters are N_H = 0.95 $\pm$ 0.02 x 10^{22} cm^{-2}, Γ = 3.7 $\pm$ 0.1 and kT = 0.395 $\pm$ 0.009 keV and obtained in the 0.5-7.0 keV band. We can assume that these parameters define the quiescent state of the 1E 2259+586. Data, folded model and residuals are presented in Figure 5.2. These results are consistent with the those published by Patel et al. (2001).

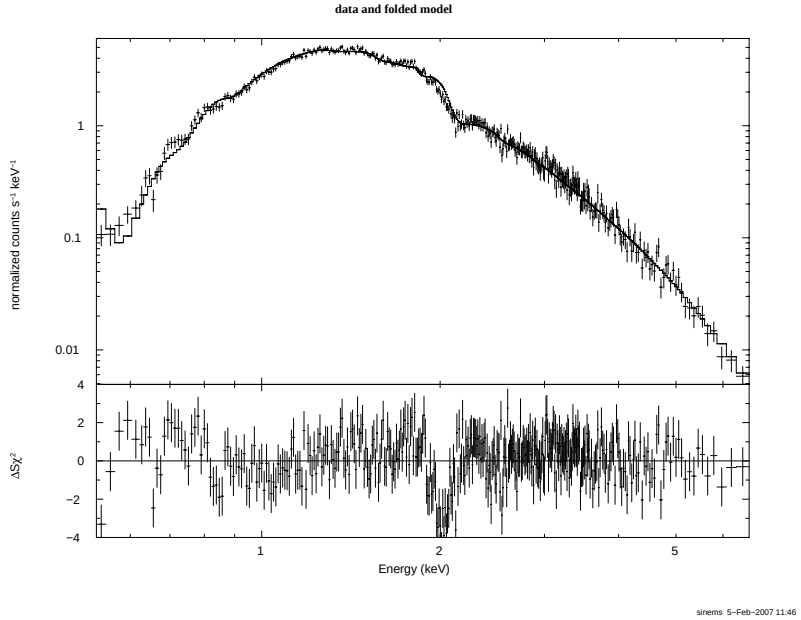

Figure 5.2: Chandra spectrum of 1E 2259+586

5.3 XMM Analysis of 1E 2259+586

Here we present the five XMM-Newton observations held on January 22, June 11 (before the outburst), June 21, 2002 (after the outburst) and, two observations on July 9, 2002. Data were taken from NASA's HEASARC archive and processed with using XMM-Newton Science Analysis System (SAS) version 7.0.0. Spectral and pulse profile changes just before, during and after the outburst are presented. Analysis presented in this section were also done by Woods et al. (2004).

5.3.1 Pulse Profiles

Pulse profiles were plotted using efold command of XRONOS v5.21. Pulse frequencies are taken from Table 2 of Woods et al., 2004 (See Table 5.1). Observations 0057540101 and 0038140101 were done before the 18 June 2002 outburst and the others were done after the outburst. Background-subtracted pulse profiles are plotted over four different energy bands. These are 0.3 - 1.0 keV, 1.0 - 2.0 keV, 2.0 - 5.0 keV, 5.0 - 12.0 keV.

Pulse profiles change over time and energy and show two maxima per cycle (See Figure 5.3). Özel (2002) showed that a hot emission region on the neutron star surface can lead to single or two peaked pulse profiles, and an antipodal geometry manifests single or up to four peaked pulse profiles determined by the general relativistic effects, orientation angles and sizes of hot regions and observer's viewing angle. Energy dependent nonradial beaming pattern of the radiation can lead to energy dependent pulse profiles and phase lags between different energy bands. Özel (2002) states that anomalous X-ray pulsars have a single emission region formed by the cracking of the crust, decay of magnetic multipoles, magnetic field reconfiguration or the viewing constraints which lead to unobservable magnetic pole or the dipole field configuration such as two closer magnetic poles.

Table 5.1: Pulse Frequencies

Observation ID	Epoch (MJD)	Frequency (Hz)[a]	Exp.Time (ks)
0057540101	52296.78969	0.14328688	7.26
0038140101	52436.41157	0.14328705	26.0
0155350301	52446.44985	0.14328746	17.0
0057540201	52464.3694	0.14328771	5.77
0057540301	52464.6059	0.14328771	10.4

[a] Woods et al. 2004

5.3.2 Spectroscopy

XMM-Newton observed 1E 2259+586 five times in 2002. We plotted a high energy light curve to determine and eliminate the flaring particle background. Spectra and background were extracted from a circle with a radius of 25 arcsec and 40 arcsec for small window-mode observations, respectively. For extended frame mode observations 40 arcsec for the pulsar and 50 arcsec for the background were extracted with using SAS command EVSELECT. Spectra were grouped to a minimum of 25 counts per bin and fitted well with blackbody plus power law model modified by interstellar absorption with using XSPEC version 12.3.1 (see Figure 5.4 and 5.5). A systematic error of 3% was used in fitting the data of ObsID 0155350301. We also tried different models such as single power law model, two blackbody model and single blackbody model modified by interstellar absorption (Figure 5.6). But these models give statistically unacceptable χ^2 values. Two blackbody model fits well below the

8 keV but above this value model does not give acceptable results. Spectral fits were restricted to the range 0.6-12.0 keV. The measured absorbed flux before the outburst is 1.27 x 10^{-11} ergs cm^{-2}s^{-1} and after the outburst is 3.39 x 10^{-11} ergs cm^{-2}s^{-1} over the range 2.0-10.0 keV. Best fit parameters are presented in Table 5.2.

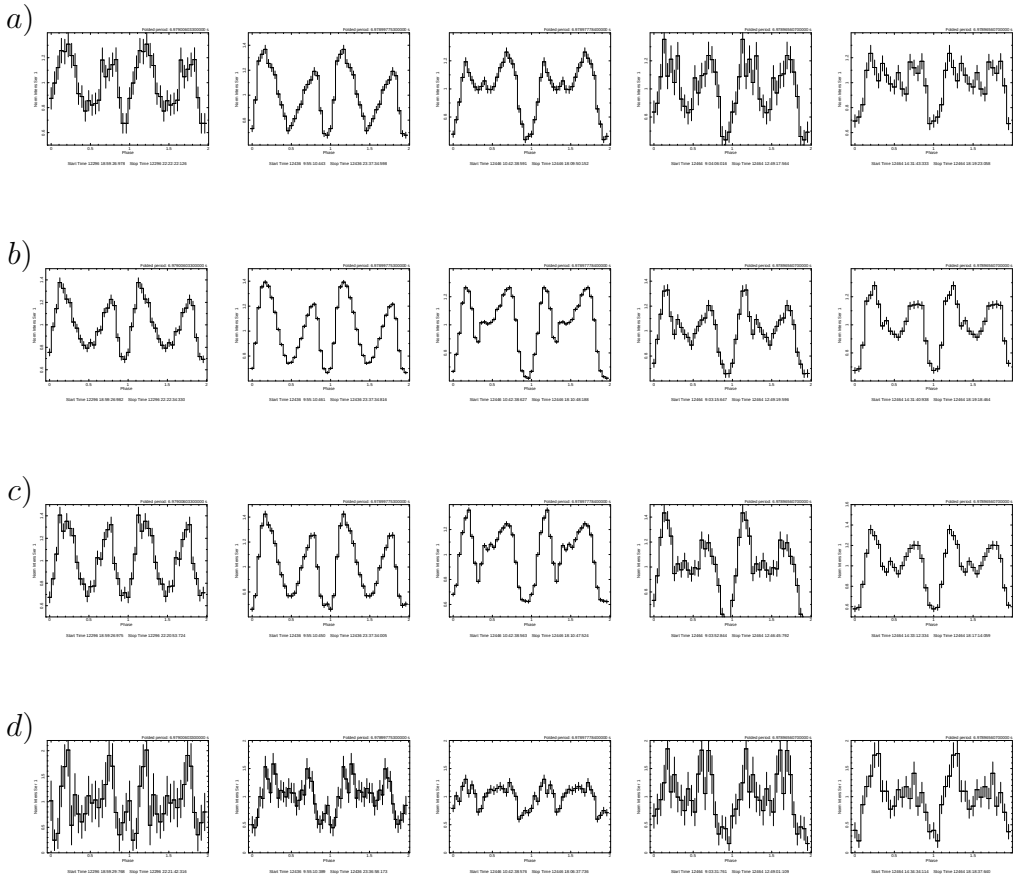

Figure 5.3: Abscissa refers to the pulse phase and ordinate refers to the normalized rate. Five columns represent the five observations with the given ObsIDs in Table 5.2 and each row represents the different energy bands. a) 0.3 - 1.0 keV b) 1.0 - 2.0 keV c) 2.0 - 5.0 keV d) 5.0 - 12.0 keV

Table 5.2: Spectral Parameters for XMM-Newton EPIC PN observations

Observation ID	N_H 10^{22} cm^{-2}	Powerlaw Index	Bbody Temp. (keV)	Unabs. Flux[a] 10^{-11} ergs $cm^{-2}s^{-1}$	χ^2/dof
0057540101	1.091±0.044	4.13±0.15	0.506±0.033	1.62±0.32	512.02/482
0038140101	0.963±0.018	3.96±0.05	0.410±0.005	1.55±0.18	898.65/847
0155350301	0.920±0.015	3.49±0.04	0.518±0.008	4.03±0.26	948.35/1035
0057540201	0.944±0.038	3.67±0.13	0.566±0.041	2.53±0.47	511.89/490
0057540301	0.905±0.028	3.57±0.09	0.559±0.022	3.14±0.39	613.72/648

[a] Unabsorbed flux over 2.0-10.0 keV.

5.3.3 Pulse-phase Spectroscopy

We performed pulse-phase spectroscopy only on ObsID 0038140101 (7 days prior to the outburst) and 0155350301 (3 days after the outburst). For extended-full frame mode, observations are statistically unacceptable to obtain phase-resolved spectrum. Data were divided into 20 phase intervals. Column density was fixed to values similar to phase-averaged values. Extracted spectra were grouped to a minimum of 25 counts per bin and fitted with blackbody plus power law model modified by interstellar absorption. Profiles and obtained spectral parameters with respect to pulse phase were shown in Figure 5.7a and 5.7b. Variation in the photon index with respect to the pulse phase before the burst which was mentioned by Woods et al. (2004) can be seen from Figure 5.7a.

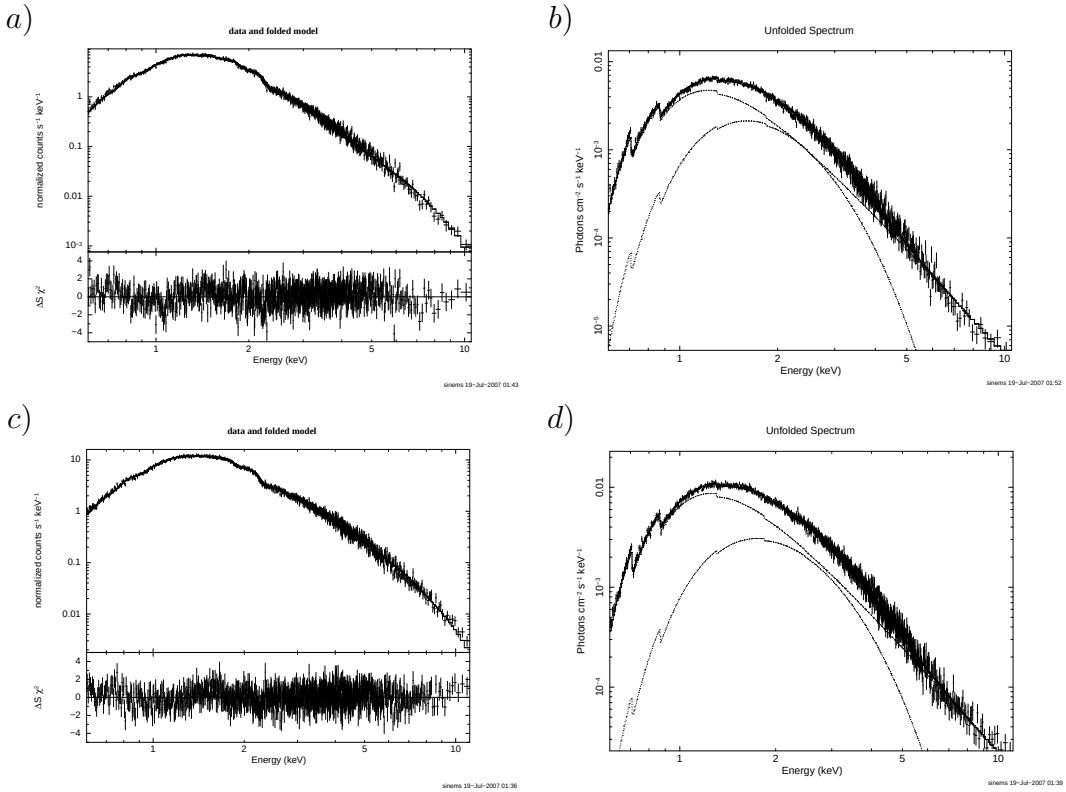

Figure 5.4: a) XMM-Newton EPIC PN phase-averaged X-ray spectrum of the ObsID 0038140101 with best fit spectral model (PL+BB) and residuals b) model c) XMM-Newton EPIC PN X-ray spectrum with best spectral fit to the ObsID 0155350301 and residuals d) model

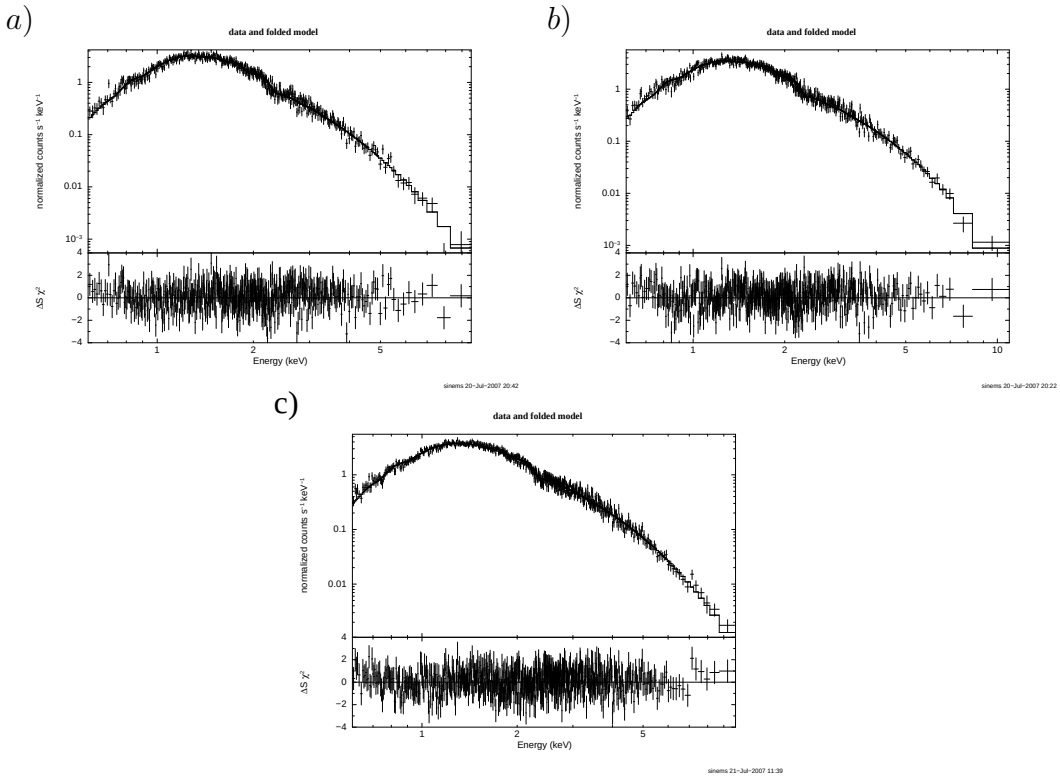

Figure 5.5: a) XMM-Newton EPIC PN phase-averaged X-ray spectrum of the ObsID 0057540101, b) 0057540201 and c) 0057540301 with best fit spectral model (PL+BB) and residuals

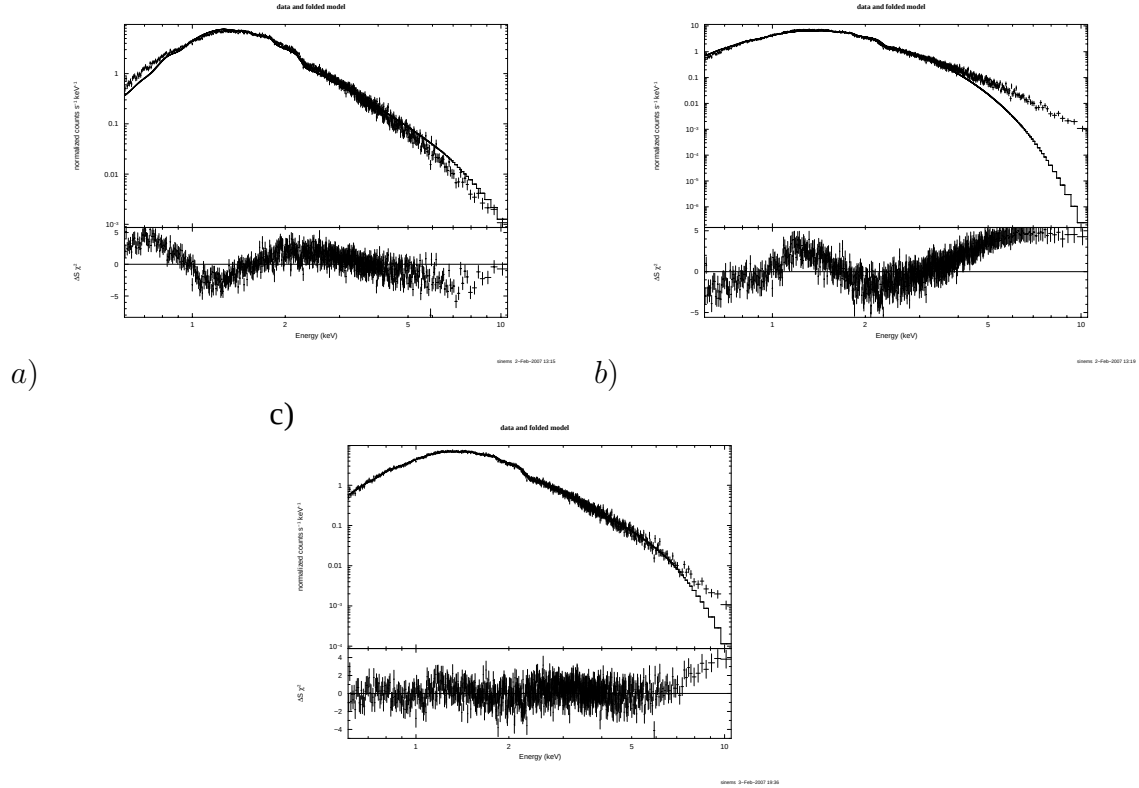

Figure 5.6: Fitted models to the ObsID 0038140101 with unacceptable statistics. a) Single power-law model b) Two blackbody model c) Single blackbody model

5.4 RXTE Observations

Results presented here are obtained using the PCA detector and data mode Standard 2 which has a time resolution of 16 s and 129 energy channels (Appendix F: XTE Technical Appendix). We analyzed 98 observations spanning over December 1996 to February 2006. Firstly, we have to model background contributions from variety of sources such as supernova remnant CTB 109 and Galactic ridge in the large field of view of RXTE and instrumental background. Instrumental background was modeled by using the PCABACKEST command and PCA background models developed by PCA team. Following Woods et al. (2004) we extract a spectrum without selecting PCU0 because of the loss of its propane layer. We used 4 May 2002 RXTE PCA

observation to model the background. Next, we fitted 4 May 2002 spectrum with blackbody plus power law model modified by interstellar absorption and plus another blackbody and a Gaussian line modified by a fixed column density of 2 x 10^{22} cm^{-2}. Spectral parameters of first blackbody and power law models were fixed to the spectral parameters obtained from XMM-Newton 11 June 2002 Observation (ObsID 0038140101). Later obtained Gaussian line and blackbody temperature were used as a cosmic background for all of the RXTE observations.

5.4.1 Pulse Frequency History and Correlation with the Long-Term Spectral Evolution

We plotted the frequency and spectral evolution before, during and after the outburst. Long-term frequency history was taken from Baykal et.al. (2007). Frequency evolution during the outburst and glitch epoch is plotted using the model taken from Woods et al. (2004).

$$\nu = \nu_0\left(t\right) + \Delta\nu + \Delta\nu_g\left(1 - e^{-(t-t_g)/\tau_g}\right) - \Delta\nu_d\left(1 - e^{-(t-t_g)/\tau_d}\right) + \Delta\dot{\nu}t \quad (5.1)$$

ν_0(t) represents the frequency evolution before the glitch, $\Delta\nu$ is the frequency jump, τ_g is the timescale of the exponentially growing frequency jump $\Delta\nu_g$, τ_d represents the timescale of the exponential frequency drop after the glitch, t_g is the glitch epoch, and $\Delta\dot{\nu}$ represents the long-term frequency derivative change after the glitch (See Table 5.3 for the model parameters). Figure 5.8 displays the model used to plot frequency evolution according to the equation 5.1 and 5.2 during the outburst and glitch. Frequency derivative is modeled with the time derivative of the equation 5.1.

$$\dot{\nu} \;=\; \dot{\nu}_0\left(t\right) + \Delta\nu_g\left(\frac{e^{-(t-t_g)/\tau_g}}{\tau_g}\right) - \Delta\nu_d\left(\frac{e^{-(t-t_g)/\tau_d}}{\tau_d}\right) + \Delta\dot{\nu} \quad (5.2)$$

In Figure 5.9 long-term frequency evolution between 4.4 $\times 10^4$ and 5.4 $\times 10^4$ MJD is presented. Figure 5.10 and 5.11 represent the spin-down evolution of zoomed region of Figure 5.9 between 5.0 $\times 10^4$ and 5.4 $\times 10^4$ MJD observed by RXTE before and after the glitch. We present the spectral evolution before outburst in Figure 5.12, after outburst in Figure 5.13 and during outburst in Figure 5.14. Power law index,

blackbody temperature and 2-10 keV unabsorbed flux variations with respect to the frequency derivative between 2002 March 22 and 2002 August 23 are presented in Figure 5.15, 5.16 and 5.17 respectively.

Table 5.3: Spin Parameters

Parameter	Value
Spin frequency,ν	0.14328703257 (21) Hz
$\dot{\nu}$	-9.920 (6) $\times 10^{-15}$ Hz s^{-1}
Epoch	52,400.0000 MJD TDB
$\Delta\nu$	5.25 (12) $\times 10^{-7}$ Hz
$\Delta\nu_g$	$> 8.7 \times 10^{-7}$ Hz
τ_g	14.1 (7)
$\Delta\nu_d$	$\Delta\nu_g$ + (5 $\times 10^{-9}$) Hz
τ_d	15.9 (6) days
$\Delta\dot{\nu}$	+2.18 (25) $\times 10^{-16}$ Hz s^{-1}
t_g	52,443.13 (9) MJD TDB
rms timing residual	44.9 ms
Start observing epoch	51,613 MJD
End observing epoch	52,900 MJD

Numbers in parentheses represent the 1 σ uncertainties in the least significant digit.

Lower limit of $\Delta\nu_g$ is given at 90 $\%$ confidence.

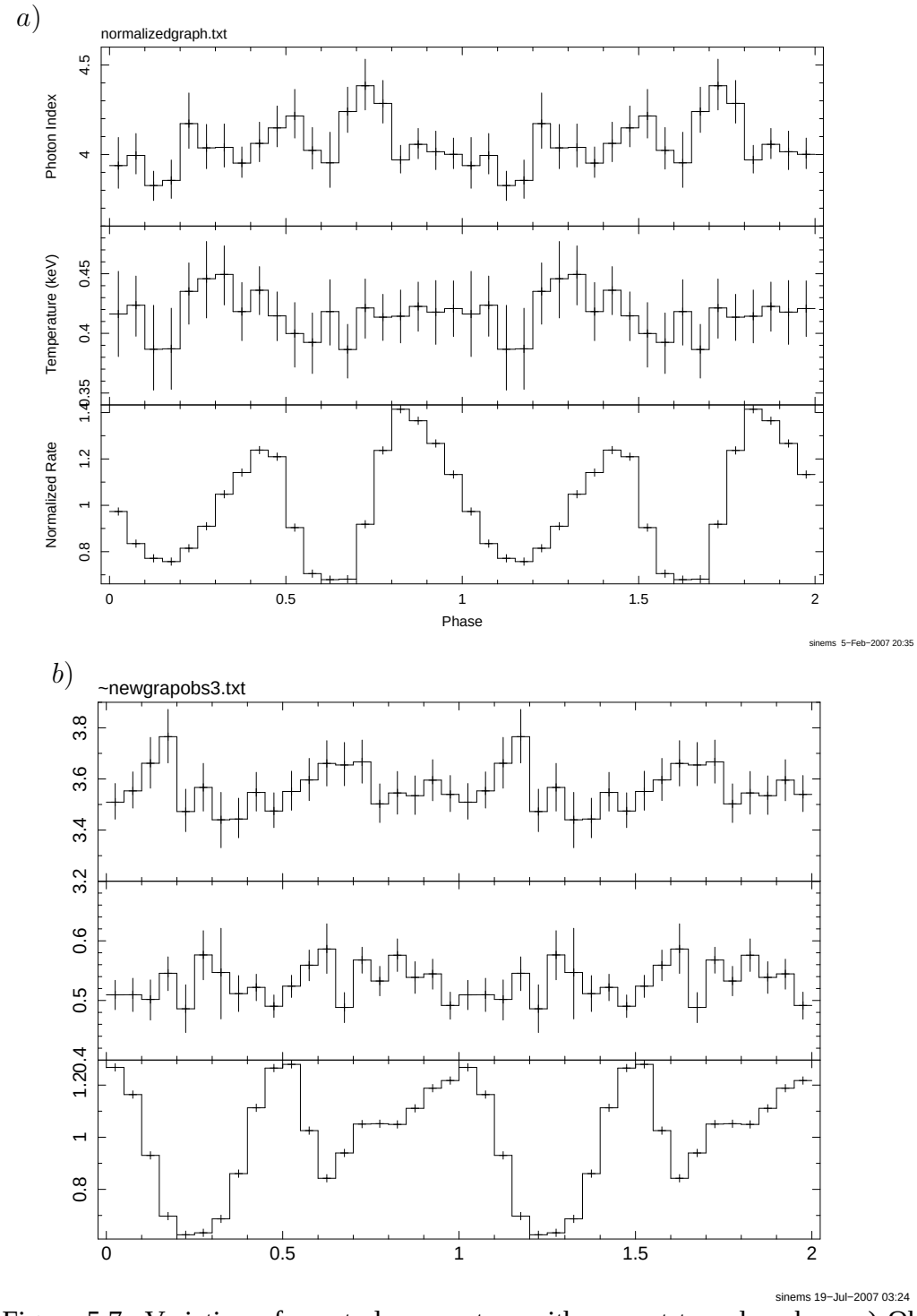

Figure 5.7: Variation of spectral parameters with respect to pulse-phase a) ObsID 0038140101 and b) 0155350301. For each figure top graphic is photon indices, middle is blackbody temperature and bottom is folded pulse profile over the energy range 0.5-7.0 keV.

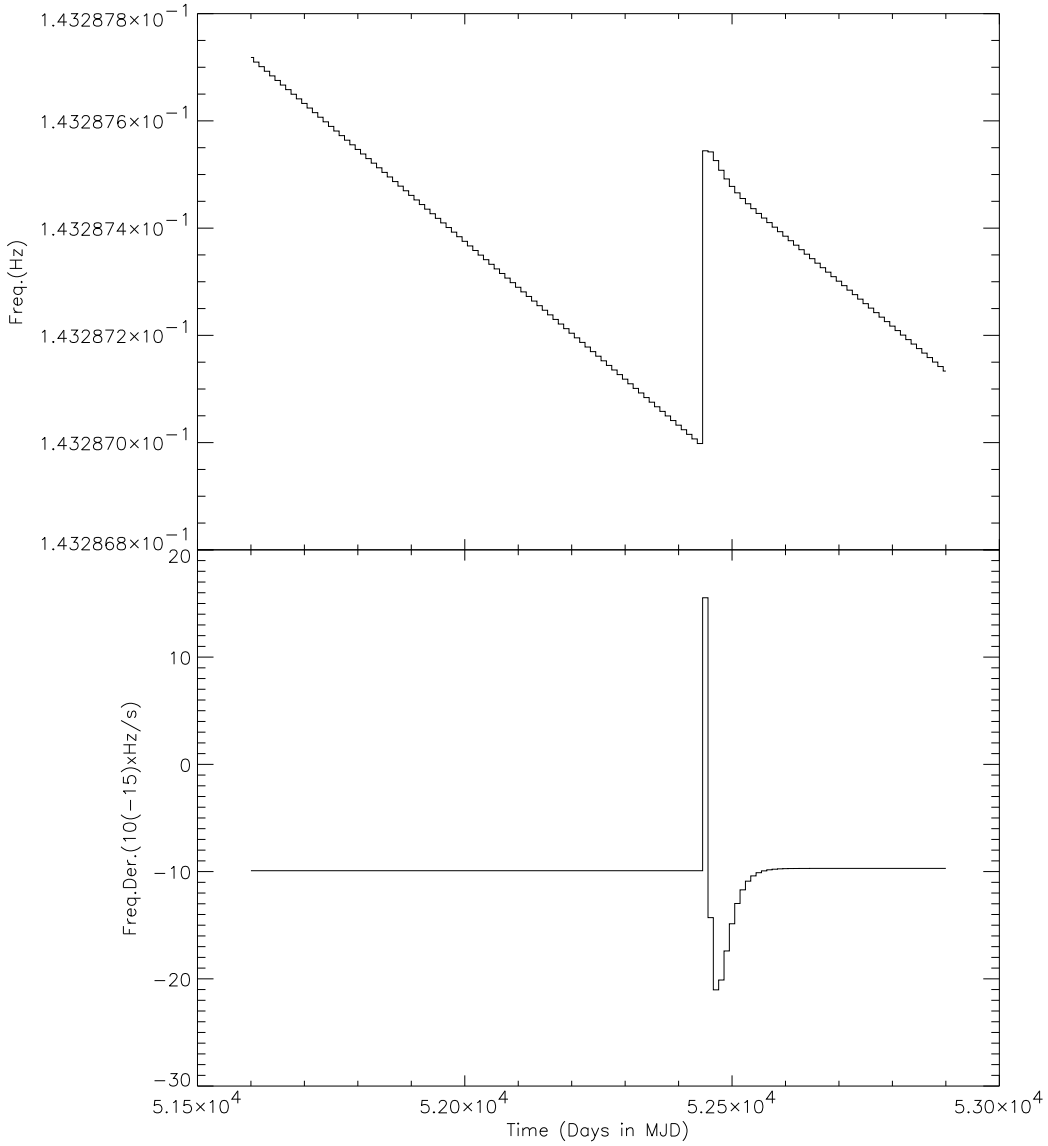

Figure 5.8: Figure represents the model used to plot frequency evolution according to the equations 5.1 and 5.2 during the outburst and glitch.

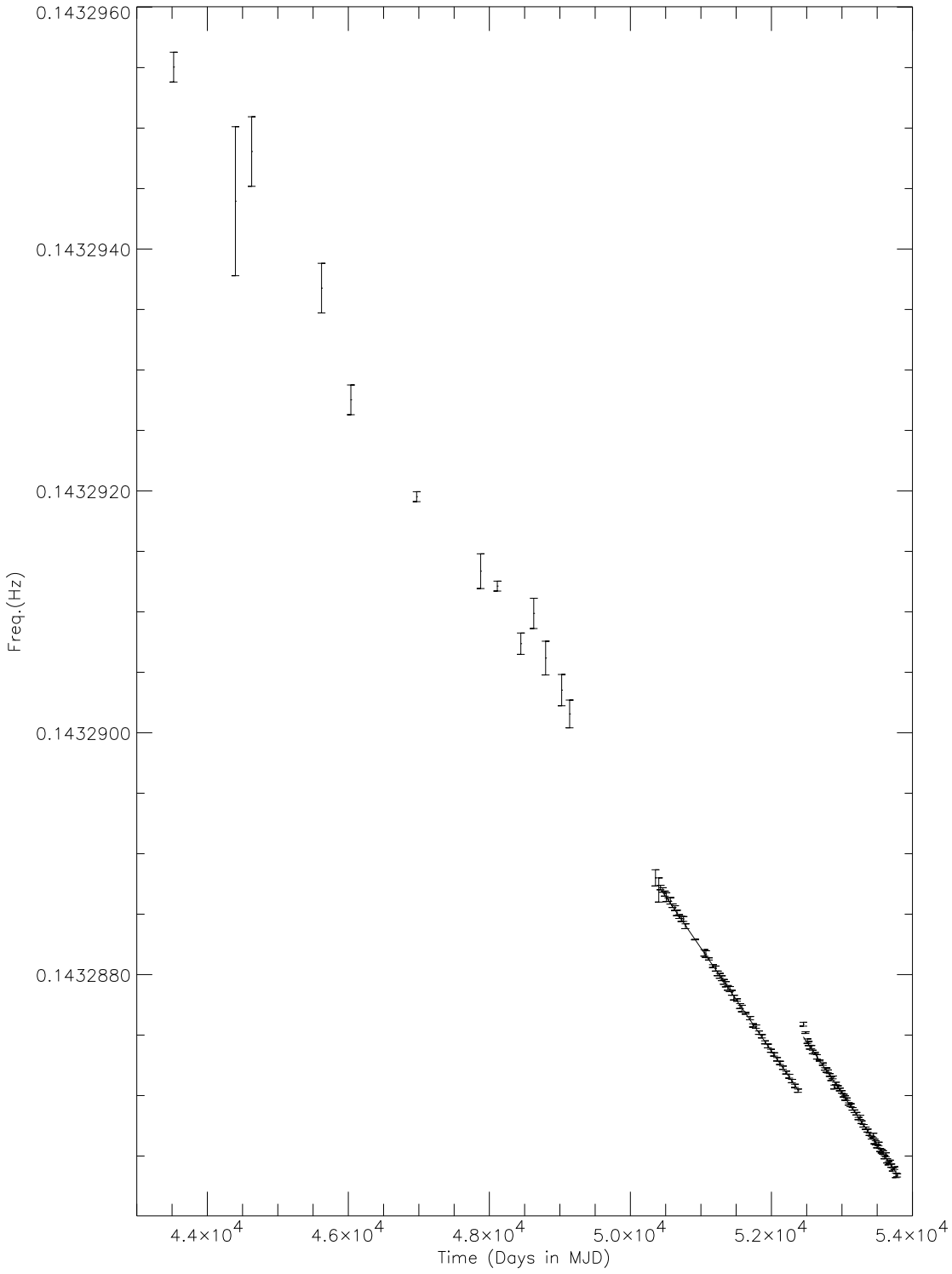

Figure 5.9: Long term frequency evolution

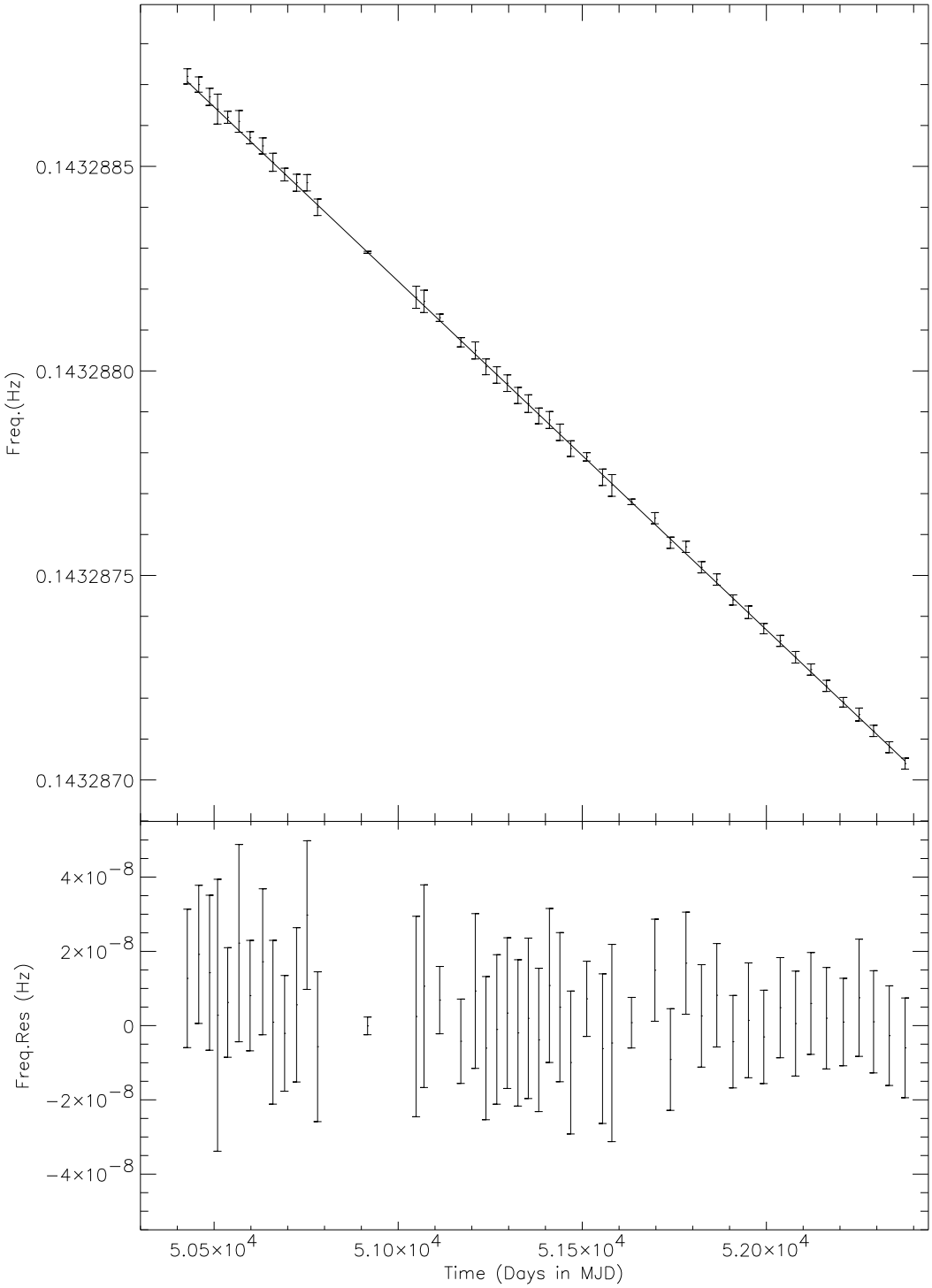

Figure 5.10: Frequency evolution before glitch

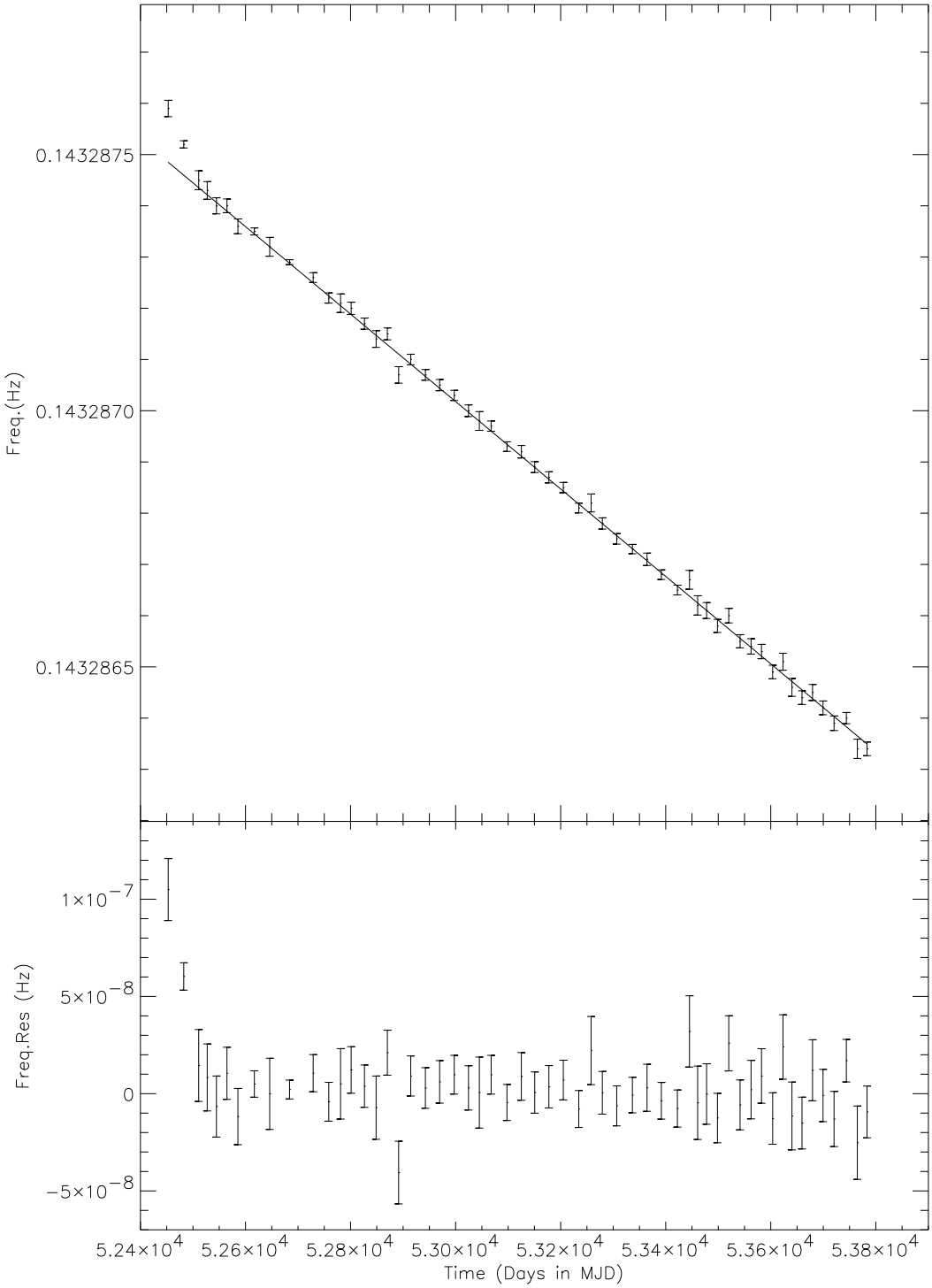

Figure 5.11: Frequency evolution after glitch

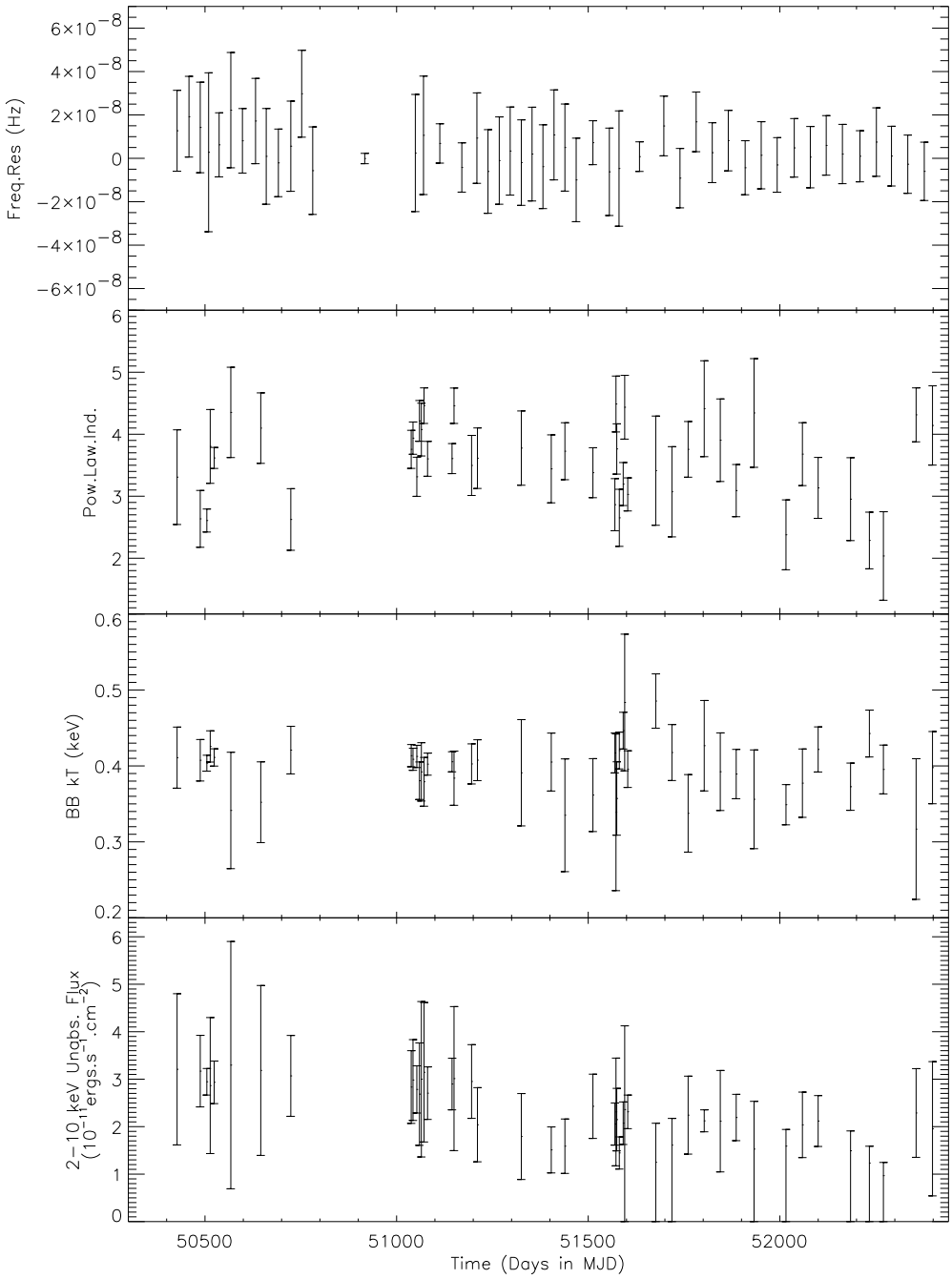

Figure 5.12: Evolution of spectral parameters before the outburst

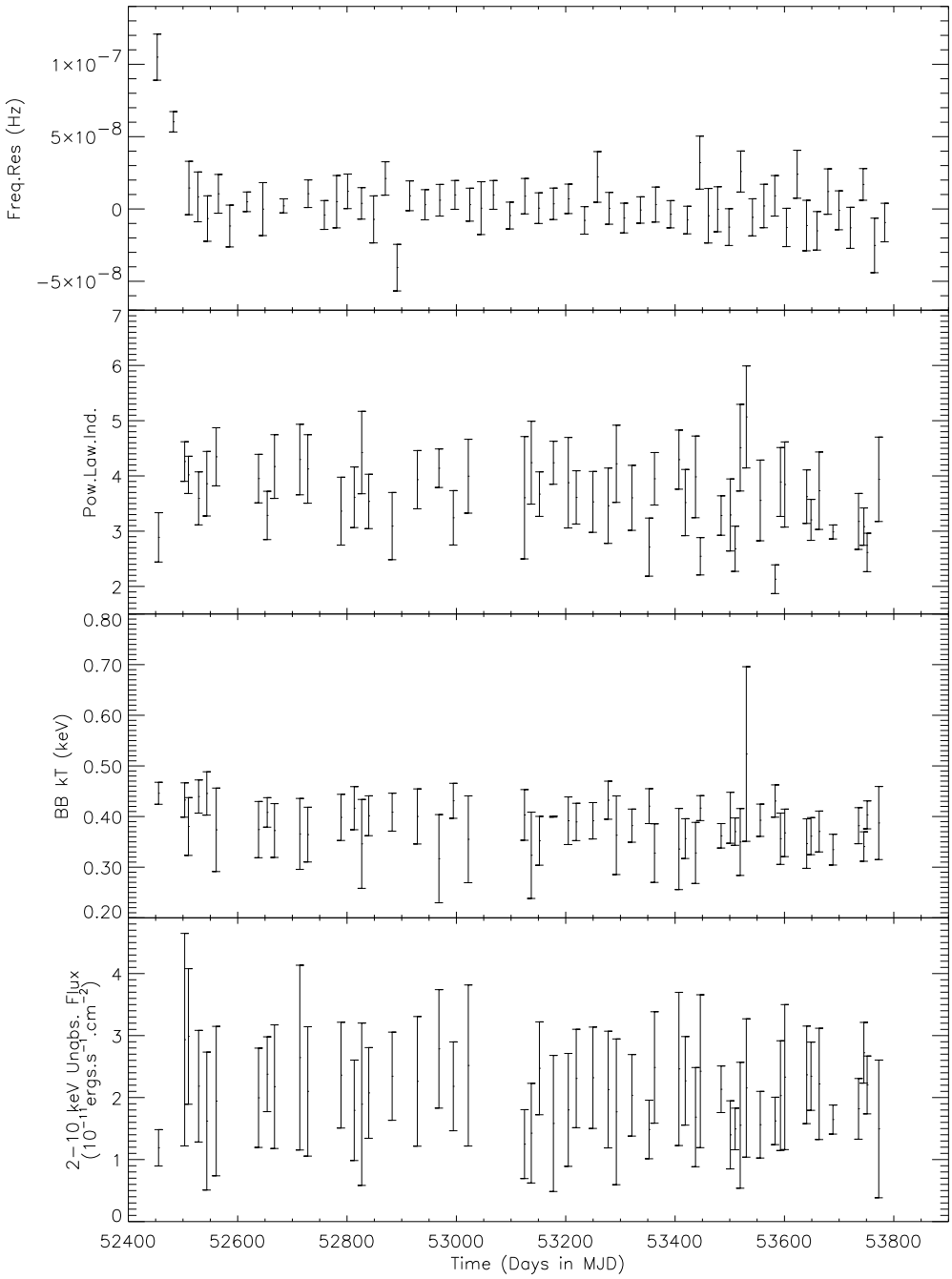

Figure 5.13: Evolution of spectral parameters after the outburst

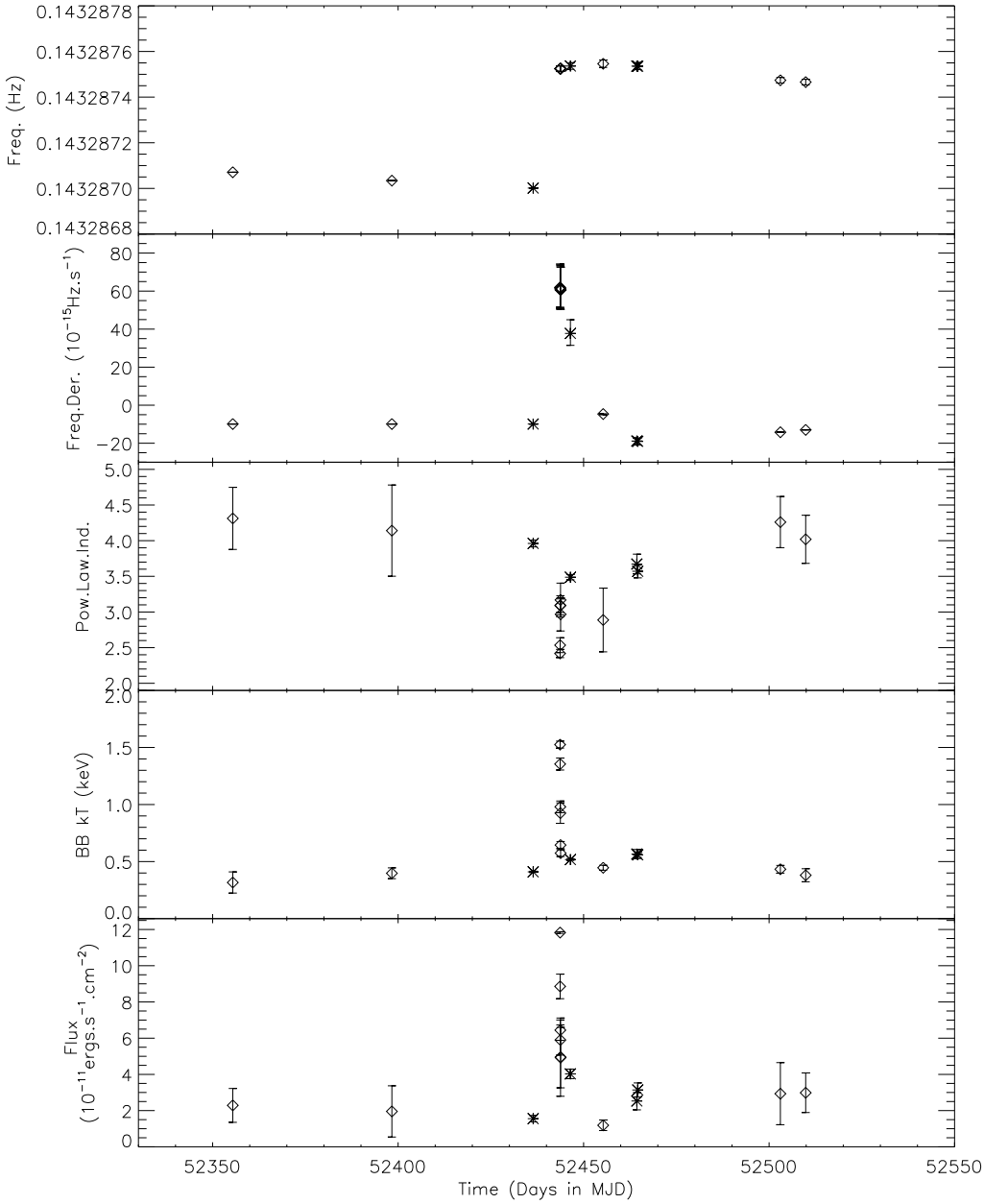

Figure 5.14: Variation of spectral parameters in the vicinity of the outburst. Star symbols represent the XMM-Newton observations and the others are RXTE observations.

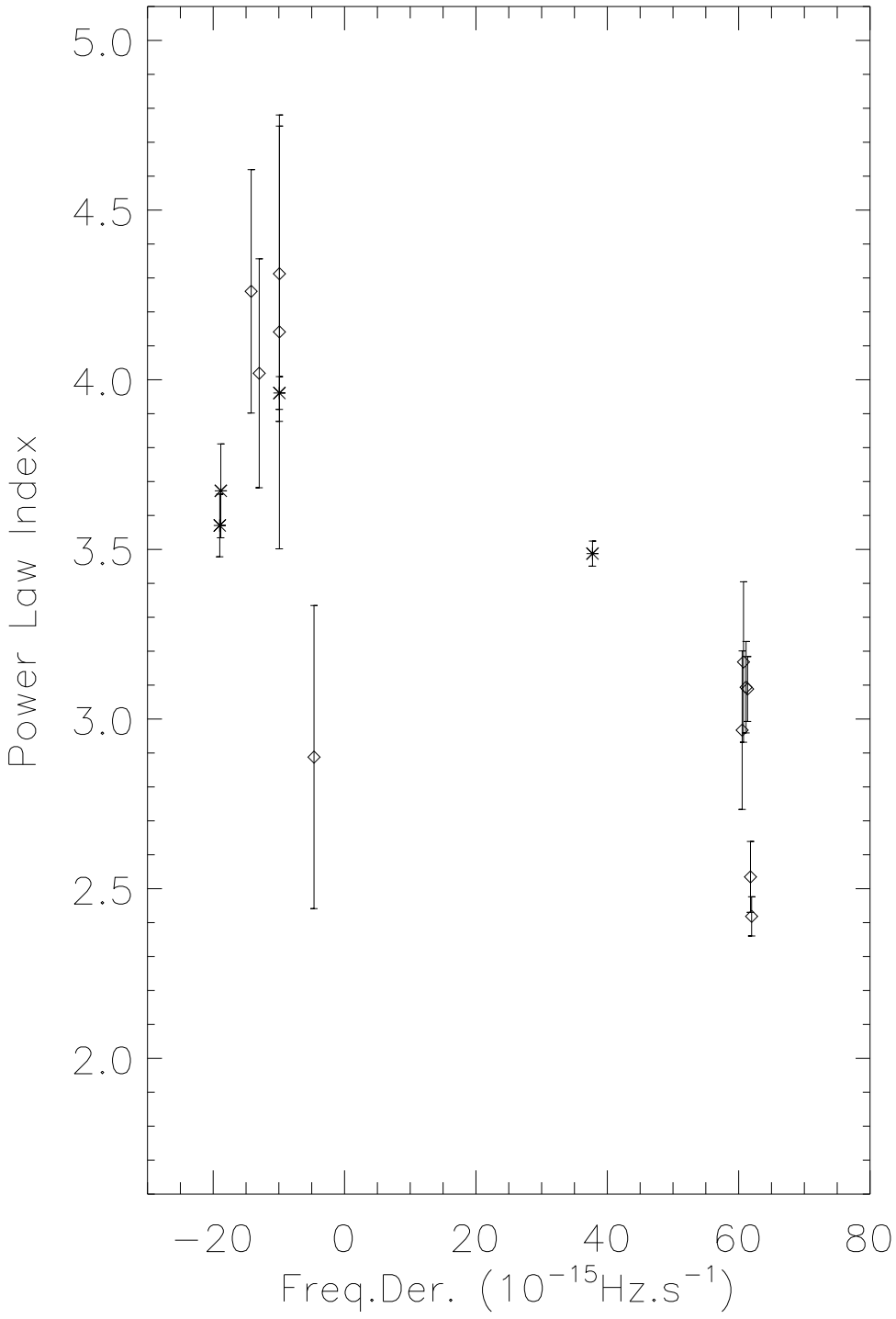

Figure 5.15: Power-law index variation with respect to the frequency derivative between 2002-03-22 and 2002-08-23. Star symbols represent the XMM-Newton observations and the others are RXTE observations.

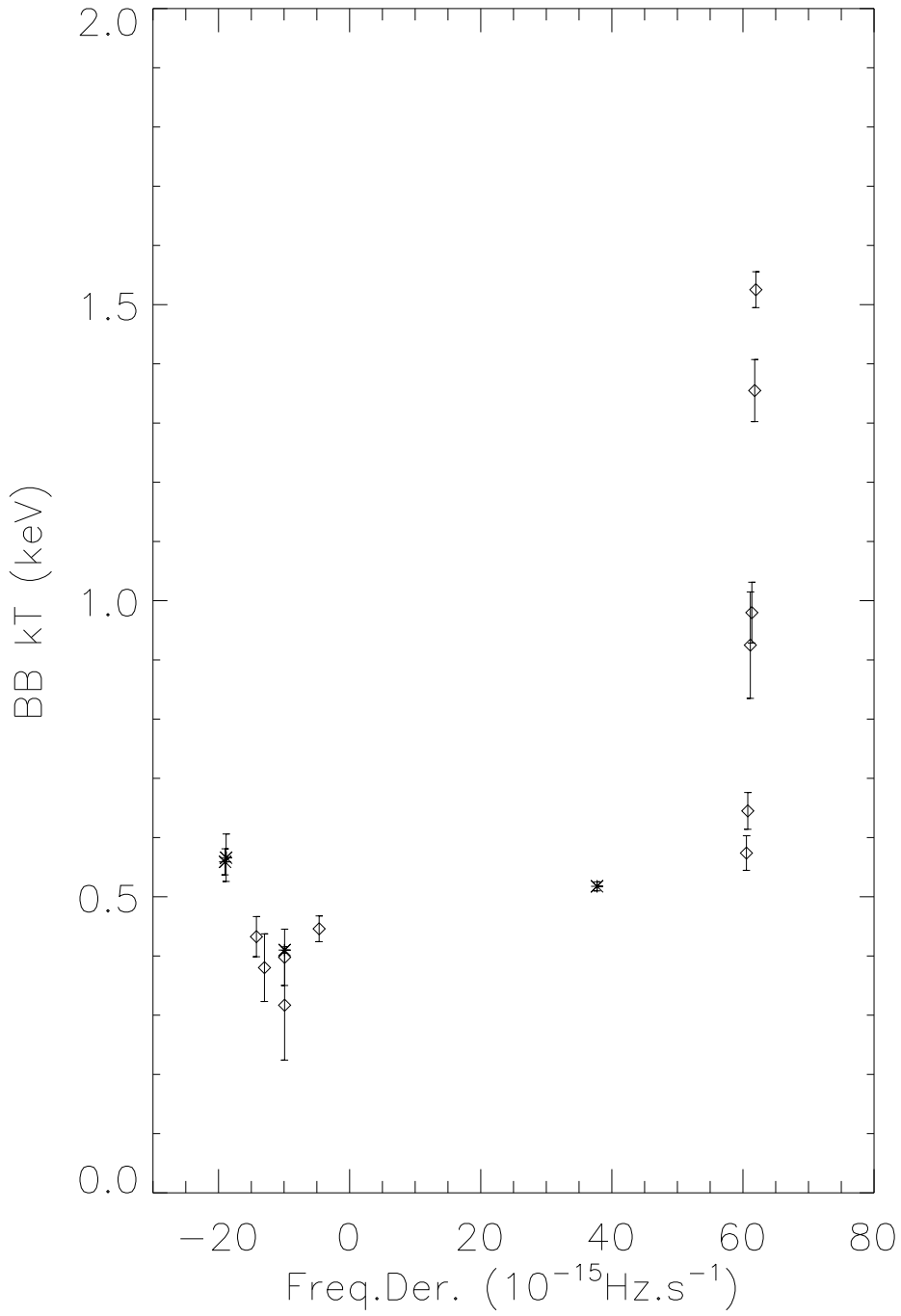

Figure 5.16: Blackbody temperature variation with respect to the frequency derivative between 2002-03-22 and 2002-08-23. Star symbols represent the XMM-Newton observations and the others are RXTE observations.

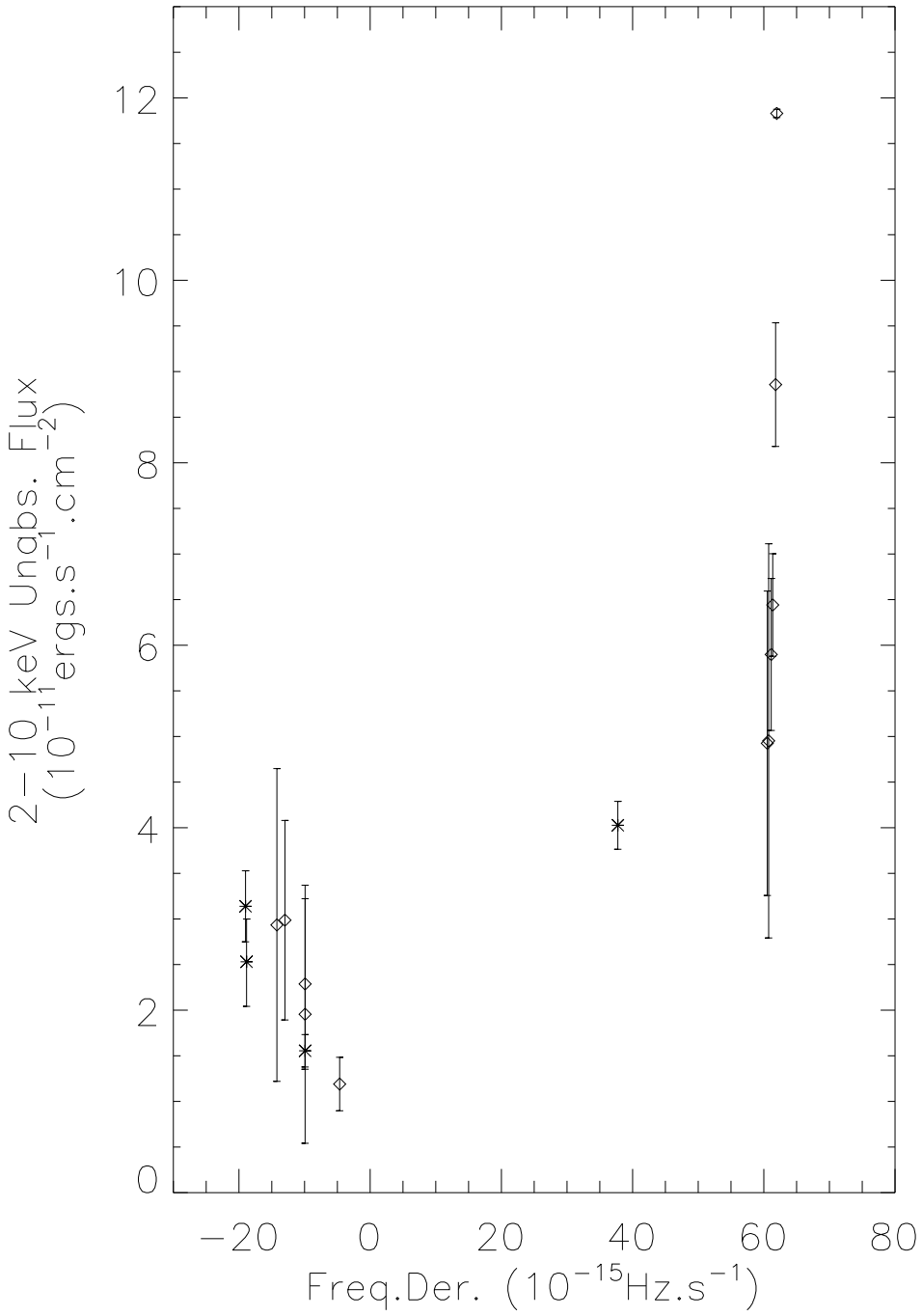

Figure 5.17: 2.0 - 10.0 keV flux variation with respect to the frequency derivative between 2002-03-22 and 2002-08-23. Star symbols represent the XMM-Newton observations and the others are RXTE observations.

CHAPTER 6

DISCUSSION AND CONCLUSION

Anomalous X-ray pulsars (AXPs) and soft gamma ray repeaters (SGRs) have spin periods in the range of 6-12 seconds. Although rapid spin-down rates have been observed, persistent spin-up episode was a part of a missed glitch event. Most of the SGRs and AXPs are associated with supernova remnants (Marsden et al, 2001). They lack Doppler shifts associated with binary orbital motion (Mereghetti, Israel and Stella 1998; Kaspi, Chakrabarty and Steinberger 1999; Baykal et al., 1998) which implies that SGRs and AXPs are not members of HMXRBs. Systems with low mass companions of less than 1 $M_{\odot}$ and Thorne-Zytkov objects are not also consistent for these sources (Ghosh, Angelini and White 1997). SGRs and AXPs have also differences, SGRs occasionally emit multiple bursts of gamma rays which have unique behavior distinguishing them from other bursting sources (Kouveliotou et al. 1993).

AXPs have softer X-ray spectra and persistent X-ray emission (Stella, Israel and Mereghetti 1998). Theoretical models describing SGRs and AXPs can be divided into two major categories based on the energy source of X-ray and gamma ray emission mechanisms. The magnetar model (Duncan and Thompson 1992) suggests that the X-ray emission and rapid spin down of SGRs and AXPs are due to the an usually strong magnetic field ($B > 10^{15}$ Gauss), which can decay on a $\sim 10^3 - 10^4$ years timespan and supply the observed X-ray emission. As for the fall back disk models (or accretion based models), Chatterjee, Hernquist and Narayan 2000 and Alpar (2001) suggests that AXPs are normal neutron stars with conventional mag-

netic fields of $\sim 10^{12}$ Gauss and their spin-down and X-ray luminosities are due to accretion of material from a fossil disk formed from supernova ejection.

Marsden and White (2001) investigated common properties of X-ray spectra of AXPs and SGRs, using the archival ASCA data over the energy range 0.5-10 keV. They studied the correlation between spectral parameters of persistent emission and spin-down rates. Using a single power law model they found that the overall hardness of the spectra increase with increasing spin down rate. They also used two component models consisting of blackbody and power law components. In this case, correlation between hardness of the high energy component with increasing spin down rate was found. However the temperature of the low energy black body component did not vary significantly. For the two component model, the ratio of the 2-10 keV power-law luminosity and bolometric blackbody luminosity gradually increased with spin down rate (see Figures 1 and 2 in Marsden and White (2001)). These observed correlations can be used to distinguish the models for SGRs and AXPs from accreting systems. With respect to the accretion model, the spectra of known accretion powered pulsars in X-ray binaries (XRBs) are generally harder than the AXP and SGR spectra over the energy range 0.5-10 keV (White, Swank and Holt 1983). XRBs have not shown correlation between spectral parameters and the spin down rates. If the AXPs and SGRs are accretion powered, then they should have clearly different spectral parameters.

In this thesis XMM-Newton, RXTE and CHANDRA analysis of anomalous X-ray pulsar 1E 2259+586 were presented. XMM-Newton observations, RXTE observations around the outburst and Chandra observations were analyzed also by Woods et al. 2004 and Patel et al. 2001 respectively and we reached similar results. We analyzed five XMM-Newton observations to present the variations just before and after the outburst. Pulse profiles were plotted in four different energy bands. Pulse profiles show energy and time variabilities, two maxima per cycle and differ from those other bursting AXPs 1E 1048.1-5937 and XTE J1810-197 which have quasi-sinusoidial profiles (Gavriil et al. 2006). Pulse phase spectroscopy was performed on two XMM-Newton observations (0038140101 and 0155350301). 0038140101 observa-

tion shows significant photon index versus pulse phase variation while 0155350301 observation shows no significant change (Figure 5.7)

We examined 98 observations spanning over December 1996 to February 2006. However, except around 2002 June 18 outburst no significant spectral and spin rate variabilities were seen (Figures 5.12, 5.13 and 5.14).

In order to see the evolution of spectral parameters of 1E 2259+586 and compare these parameters with spin rate changes, we extracted all archival RXTE, XMM and Chandra observations. We employed two component X-ray spectral fits. We present our XMM and RXTE spectral results near the glitch as a function of spin rate. We have seen that a correlation exists between power law index and spin rate. X-ray spectra gets harder (i.e. power law index decreases) as the spin rate increases (Figure 5.15).

We have seen a systematic increase in the blackbody temperature with the spin rate. This correlation is presented in Figure 5.16. Changes of spin rate coincide with the outburst and glitch activity. Definitely blackbody temperature is increased during the outburst. It should also be noted that in HMXRB source SAX J2103.5+4545, spectra changes have been observed with increasing X-ray flux (Baykal et al., 2007). However in this source as the X-ray flux increases the X-ray source gets harder but the change in the power law index is between 1.3 and 1.5. For 1E 2259+586, X-ray flux increases with increasing spin rate which resembles spin-up and X-ray flux correlation in accretion powered pulsars as for the source SAX J2103.5+4545. However, dramatic change in the power law index of the source with the spin rate and a much softer X-ray spectra suggest that the emission mechanism of 1E 2259+586 and the accretion powered pulsar SAX J2103.5+4545 are entirely different.

Woods et al. (2007) found a correlation between the spectral hardness and intensity from the spectral history of SGR 1806-20 between 1993 and 2004. Campana et al. (2006) and Rea et el. (2006) presented the intensity-hardness correlation of AXP 1RX J170849.0-400910 between 2004 and 2005, and the same correlation was observed in SGR 1900+14 before the August 1998 giant flare (Tiengo et al. 2006). Recently, Özel and Güver (2007) studied hardness-intensity correlations within the

framework of a thermally emitting magnetar model. Their atmosphere models predict that the hardness of the spectra is correlated with the surface temperature and X-ray flux. Our spectral fits around the outburst region also shows that an increase in X-ray flux is accompanied with an increase in hardness (decreasing photon index) and an increase in blackbody temperature. Özel & Güver proposed several mechanisms to explain the observed correlation. Among these mechanisms charged particle density changes in the magnetosphere triggered by the outburst may lead to the observed intensity-hardness correlation of 1E 2259+586.

APPENDIX A

OBSERVATION ID AND EXPOSURE LIST

LIST OF RXTE OBSERVATION IDS, DATES AND EXPOSURE TIMES USED IN THE ANALYSIS

A.1 Table 1A

ID	*Date*	*Merged*	*Exp.* (*sec*)
10192-03-01-01	50356.05149305555825		7536
10192-03-01-00	50356.9376041666655		10576
20146-01-01-00	50411.71313078703675		
		50427.2298929398148	1008
20146-01-02-00	50442.74665509259285		
20146-01-03-00	50473.8494560185209		
		50487.7103298611128	1616
20146-01-04-00	50501.580706018518		
20145-01-01-00	50504.8508506944454		13040
20145-01-01-01	50506.49695601852		6736
20145-01-02-00	50513.7094849537025		4960
20145-01-04-00	50523.8550115740727		
20145-01-04-01	50524.0266782407416	50524.0431346450604833	24032
20145-01-04-02	50524.24771412036715		
20145-01-05-01	50532.19444444444525		
		50532.58340277777825	14512
20145-01-05-00	50532.97236111111125		
20146-01-06-00	50556.58278935185445		
		50567.472508680555625	1584
20146-01-07-00	50578.3622280092568		
20146-01-08-00	50617.27270833333025		
20146-01-09-00	50646.70434606481645	50645.638177083333467	2224
20146-01-10-00	50672.9374768518537		
20146-01-11-00	50710.084184027779		
		50724.001021412037525	1472
20146-01-12-00	50737.91785879629605		

A.2 Table 1A-Continuing

ID	$Date$	$Merged$	$Exp.$ (sec)
30126-01-01-00	51038.1847106481509		13456
30126-01-02-00	51042.8231712962988		14832
30126-01-04-00	51052.79521990740615		10576
30126-01-05-00	51059.6215046296311		10144
30126-01-06-00	51064.6062152777777		4816
30126-01-07-00	51071.63766203703565		12898
30126-01-08-00	51080.8216435185204		13008
30126-01-09-00	51144.7131828703714		15136
30126-01-10-00	51149.8069502314829		12496
40083-01-01-00	51195.5949247685203		
		51195.66274594907555	7552
40083-01-02-00	51195.7305671296308		
40083-01-03-00	51198.50521412036685		
		51210.96089120370195	5568
40083-02-01-00	51223.41656828703705		
40083-02-04-00	51310.6900983796295		
		51325.375402199073525	5536
40083-02-05-00	51340.06070601851755		
40083-02-07-00	51396.82607638888655		
40083-03-01-00	51405.03983796296235		
		51403.5356495949054	10020
40083-03-02-00	51405.1749942129609		
40083-03-03-00	51407.1016898148118		
40083-02-08-00	51424.7371122685181		
		51439.14158854166635	6144
40083-02-09-00	51453.5460648148146		

A.3 Table 1A-Continuing

ID	$Date$	$Merged$	$Exp.$ (sec)
40083-02-10-00	51483.6066550925934		
		51512.17953124999985	4944
40083-02-12-00	51540.7524074074063		
40082-01-01-00	51569.48816550925765		7776
40082-01-02-00	51572.2970370370349		
40082-01-02-01	51572.3877835648127		
		51572.35858434606325	10180
40082-01-02-02	51572.45653356481485		
40082-01-02-03	51572.53917245370395		
40082-01-02-04	51574.2804398148146		
40082-01-02-05	51574.38221643518775		
		51574.34990017361133	8560
40082-01-02-06	51574.4506192129629		
40082-01-02-07	51574.564166666667		
40082-01-03-01	51581.07145833333195		
		51581.145792824072475	10380
40082-01-03-00	51581.220127314813		
40082-01-04-00	51591.24980902778045		14340
40082-01-05-00	51595.17900462963005		9088
40082-01-06-00	51603.1146701388898		12980
40082-01-07-00	51616.47663773148085		8000
40082-01-08-00	51630.07434606481545		5888
50082-01-01-00	51613.82280092592555		6064
50082-01-02-00	51676.22664351851925		6944

A.4 Table 1A-Continuing

ID	$Date$	$Merged$	$Exp.$ (sec)
50082-01-03-00	51718.2175231481488		
50082-01-03-01	51718.28374421296395	51718.310007716050083	5424
50082-01-03-02	51718.4287557870375		
50082-01-04-00	51760.5910358796282		6560
50082-01-05-00	51802.67076967592585		6448
50082-01-06-00	51844.61334490740775		6176
50082-01-07-00	51886.13542824074105		6240
50082-01-08-00	51932.62512152777705		7232
60069-01-01-00	52016.0244212962971		6704
60069-01-02-01	52058.85306134259005		
		52058.907607060184075	7376
60069-01-02-00	52058.9621527777781		
60069-01-03-00	52099.84843750000075		
		52099.898313078703725	6688
60069-01-03-01	52099.9481886574067		
60069-01-04-00	52142.08134837962645		7248
60069-01-05-00	52184.42447916666785		7120
60069-01-06-00	52233.53116319444235		6560
60069-01-07-00	52270.19783564814865		5456
60069-01-08-00	52312.2246817129635		5984
70094-01-01-00	52355.32439814815005		
		52355.4434548611116	6976
70094-01-01-01	52355.56251157407315		
70094-01-02-01	52398.2315972222204		
70094-01-02-02	52398.3031249999985	52398.3217573302463	7584
70094-01-02-00	52398.43054976852		

A.5 Table 1A-Continuing

ID	$Date$	$Merged$	$Exp.$ (sec)
70094-01-03-01	52445.05885416666935		
		52445.100616319447	8864
70094-01-03-02	52445.14237847222465		
70094-01-04-00	52449.323645833334		2448
70094-01-05-00	52455.04773726851635		
70094-01-05-01	52455.1940972222219	52455.276203703702783	10640
70094-01-05-02	52455.5867766203701		
70094-01-06-00	52503.0497395833336		9120
70094-01-07-00	52509.8703877314838		6064
70094-01-09-00	52528.5906655092585		5840
70094-01-11-00	52543.4766319444425		6928
70094-01-14-00	52560.7498263888883		6496
70094-01-15-00	52568.5296817129638		6336
70094-01-16-00	52575.51589120370045		6608
70094-01-17-00	52595.52267361111085		6608
70094-01-18-00	52638.17527777778015		7472
70094-01-19-00	52653.97535879629505		6256
70094-01-20-00	52667.36828703703575		6352
70094-01-21-00	52686.04564814814875		5216
80098-01-02-00	52713.6716956018499		4352
80098-01-03-00	52728.2216145833299		5664
80098-01-09-00	52813.1572280092587		5424
80098-01-10-00	52826.85758101851755		4560
80098-01-11-00	52839.7385185185194		5696
80098-01-14-00	52882.5560011574089		2992

A.6 Table 1A-Continuing

ID	$Date$	$Merged$	$Exp.$ (sec)
80098-01-17-00	52928.61585648147955		5200
90076-01-03-00	53096.1106134259244		4896
90076-01-05-00	53124.5996817129635		4096
90076-01-06-00	53136.9773726851854		4800
90076-01-07-00	53151.803680555553		5200
90076-01-09-00	53177.33573495370365		
		53177.361802662037	3888
90076-01-09-01	53177.38787037037035		
90076-01-11-00	53204.6970949074057		4816
90076-01-12-00	53219.19693865740555		5616
90076-01-14-00	53249.6521006944422		4864
90076-01-16-00	53277.6514930555568		4448
90076-01-17-00	53292.5338425925911		4928
90076-01-19-02	53320.6942361111105		
90076-01-19-01	53320.9078645833324		
		53320.8986284722222875	5872
90076-01-19-00	53320.9842534722229		
90076-01-19-03	53321.00815972222335		
90076-01-21-00	53352.41929398148205		4560
90076-01-22-00	53362.2680787037025		
		53362.3033015046276	4416
90076-01-22-01	53362.3385243055527		
90076-01-25-01	53406.9940567129634		
		53407.028987268518925	4784
90076-01-25-00	53407.06391782407445		

A.7 Table 1A-Continuing

ID	$Date$	$Merged$	$Exp.$ (sec)
90076-01-26-00	53418.51647569444685		
		53418.5520891203705	3488
90076-01-26-01	53418.58770254629415		

REFERENCES

[1] Alpar, M.A., 2001, ApJ, 554, 1245

[2] Baykal, A., İnam, S.Ç., Şaşmaz, S., 2007, in preperation

[3] Baykal, A., İnam, S.Ç., Stark, M.J., Heffner, C.M., Erkoca, A.E., Swank, J.H., 2007, MNRAS, 374, 1108

[4] Baykal, A., Swank, J.H., Strohmayer, T., Strak, M.J., 1998, A&A, 336, 173

[5] Baykal, A., Swank, J., 1996, ApJ, 460, 470

[6] Camilo, F., Kaspi, V.M., Lyne, A.G., Manchester, R.N., Bell, J.F., D'Amico, N., McKay, N.P.F., Crawford, F., 2000, ApJ, 541, 367

[7] Campana, S., Rea, N., Israel, G.L., Turolla, R., Zane, S., 2006, astro-ph/0611216 v1

[8] Chandra X-ray Center, Chandra Project Science, MSFC, Chandra IPI Teams, The Chandra Proposers' Guide v9, 2006

[9] Chatterjee, P., Hernquist, L, Narayan, R., 2000, ApJ, 534, 373

[10] Chatterjee, P., Hernquist, 2000, ApJ, 543, 368

[11] Cline,T.L., Desai, U.D., Pizzichini, G., Teegarden, B.J., Evans, W.D., Klebesadel, R.W., Laros, J.G., Hurley, K., Niel, M., Vedrenne, G., Estoolin, I.V., Kouznetsov, A.V., Zenchenko, V.M., Hovestadt, D., Gloeckler, G., 1980, ApJ, 237, L1

[12] Corbet, R.H.D., Smale, A.P., Ozaki, M., Koyama, K., Iwasawa, K., 1995, ApJ, 443, 786

[13] Dall'Osso, S., Israel, G.L., Stella, L., Possenti, A., Perozzi, E., 2003, ApJ, 599, 485

[14] Duncan, R.C. & Thompson, C., 1992, ApJ, 392, L9

[15] Ehle, M., Breitfellner, M., Gonzalez R., Guainàzzi, M., Loiseau, N., Rodriguez, M., Santos-Lleò, M., Schartel, N., Tomàs, L., Verdugo, E., Dahlem, M., 2006, XMM-Newton Users' Handbook, Issue 2.4

[16] Ekşi, K.Y., Alpar, M.A., 2003, ApJ, 599, 450

[17] Jansen, F.A., ESA SP-1268, Report on the activities of the research & scientific support department 2001-2002, 2003, Scientific editor Wenzel, K.P., editor Wilson, A.,

[18] Evans W.D., Klebesadel, W.R., Laros, J.G., Cline, T.L., Desai, U.D., Pizzichini, G., Teegarden, B.J., Hurley, K., Niel, M., Vedrenne, G., Estoolin, I.V., Kouznetsov, A.V., Zenchenko, V.M., Kurt, V.G., 1980, ApJ, 237, L7

[19] Fahlman, G. G., Gregory, P. C., Sept. 17, 1981, Nature, vol. 293, 202

[20] Flowers, E., Ruderman, M.A., 1977, ApJ, 215, 302

[21] Gavriil, F.P, Kaspi, V.M., Woods, P.M., 2006, ApJ, 641, 418

[22] Gavriil, F.P, Kaspi, V.M., 2002, ApJ, 567, 1067

[23] Gavriil, F.P., Kaspi, V.M., Woods, P.M., 2002, Nature, 419, 142

[24] Ghosh, P., Angelini, L., White, N.E., 1997, ApJ, 478, 713

[25] Glasser, C.A., Odell, C.E., Seufert, S.E., 1994, IEEE Transactions on Nuclear Science, vol.41, no.4

[26] Golenetskii, S.V., Ilyinskii, V. N. Mazets E.P., 1984, Nature, 307, 41G

[27] Goldreich, P., Reisenegger, A., 1992, ApJ, 395, 250

[28] Gotthelf, E.V., Halpern, J.P., 2007, Ap&SS, 308, 79

[29] Gotthelf, E.V., Halpern, J.P., 2005, ApJ, 632, 1075

[30] Gotthelf, E.V., Halpern, J.P., 2005, ApJ, 618, 874

[31] Gotthelf, E.V., Halpern, J.P., Buxton, M., Bailyn, C., 2004, ApJ, 605, 368

[32] Gögüş, E., Kouveliotou, C., Woods, P.M., Finger, M.H., van der Klis, M., 2002, ApJ, 577, 929

[33] Ibrahim, I.A., Markwardt, C.B., Swank, J.H., Ramsom, S., Roberts, M., Kaspi, V., Woods, P.M., Safi-Harb, S., Balman, S., Parke, C.W., Kouveliotou, C., Hurley, K., Cline, T., 2004, ApJ, 609, L21

[34] Hulleman, F., Tennant, A.F., van Kerkwijk, M.H., Kulkarni, S.R., Kouveliotou, C., Patel, S.K., 2001, ApJ, 563, L49

[35] Hulleman, F., van Kerkwijk, M.H., Kulkarni, S.R., 2004, A&A, 416, 1037

[36] Hulleman, F., van Kerkwijk, M.H., Kulkarni, S.R., astro-ph/0011561 v1

[37] Hurley, K., Mochkovitch, R., 2000, Nuclear Physics B (Proc. Suppl), 80, 207

[38] Hurley, K., Li, P., Kouveliotou, C., Murakami, T., Ando, M., Strohmayer, T., van Paradijs, J., Vrba, F., Luginbuhl, C., Yoshida, A., Smith, I., 1999, ApJ, 510, L111

[39] Ibrahim, A.I., Markwardt, C.B., Swank, J.H., Ransom, S., Roberts, M., Kaspi, V., Woods, P.M., Safi-Harb, S., Balman, S., Parke, W.C., Kouveliotou, C., Hurley, K., Cline, T., 2004, ApJ, 609, L21

[40] Israel, G.L., Oosterbroek, T., Stella, L., Campana, S., Mereghetti, S., Parmar, A.N., 2001, 560, L65

[41] Israel, G.L., Oosterbroek, T., Angelini, L., Campana, S., Mereghetti, S., Parmar, A.N., Segreto, A., Stella, L., van Paradijs, J., White, N.E., 1999, A&A, 346, 929

[42] Iwasawa, K., Koyama, K., Halpern, J.P., 1992, PASJ, 44, 9

[43] Jansen, F., Lumb, D., Altieri, B., Clavel, J., Ehle, M., Erd, C., Gabriel, C., Guainazzi, M., Gondoin, P., Much, R., Munoz, R., Santos, M., Schartel, N., Texier, D., Vacanti, G., 2001, A&A, 365, L1

[44] Juett, A.M., Marshall, H.L., Chakrabarty, D., Schulz, N., 2002, ApJ, 568, L31

[45] Kaspi, V.M., Gavriil, F.P., 2003, ApJ, 596, L71

[46] Kaspi, V.M., Gavriil, F.P., Woods, P.M., Jensen, J.B., Roberts, M.S.E., Chakrabarty, D., 2003, ApJ, 588, L93

[47] Kaspi, V.M., Gavriil, F.P., Chakrabarty, D., Lackey, J.R., Muno, M.P., 2001, ApJ, 558, 253

[48] Kaspi, V.M., Lackey, J.R., Chakrabarty, D., 2000, ApJ, 537, L31

[49] Kaspi, V.M., Chakrabarty, D., Steinberger, J., 1999, ApJ, 525, L33

[50] Kern, B., Martin, C., 2002, Nature, 417, 527

[51] Kothes, R., Uyaniker, B., Yar, A., 2002, ApJ, 576, 169

[52] Kouveliotou, C., Eichler, D., Woods, P.M., Lyubarsky, Y., Patel, S.K., Gögüş, E., van Der Klis, M., Tennant, A., Wachter, S., Hurley, K., 2003, ApJ, 596, L79

[53] Kouveliotou, C., Duncan, R.C., Thompson, C., 2003 February, Scientific American, Inc.

[54] Kouveliotou, C., Strohmayer, T., Hurley, K., van Paradijs, J., Finger, M.H., Dieters, S., Woods, P., Thompson, C., Duncan, R.C., 1999, ApJ, 510, L115

[55] Kouveliotou, C.A., Fishman, G.J., C., Meegan, Paciesas, W. S., Wilson, R.B., van Paradijs, J., Preece, R.D., Briggs, M.S., Pendleton, G.N., Brock, M.N., Koshut, T.M., Horack,M., 1993, Nature, 362, 728

[56] Kuiper, L., Hermsen, W., den Hartog, P.R., Collmar, W., 2006, ApJ, 645, 556

[57] Kulkarni, S.R., Kaplan, D.L., Marshall, H.L., Frail, D.A., Murakami, T., Yonetoku, D., 2003, ApJ, 585, 948

[58] Longair, M.S., 1992, High Energy Astrophysics, Cambridge University Press

[59] Laros, J.G., Fenimore, E.E., Klebesadel, R.W., Atteia, J.L., Boer, M., Hurley, K., Niel, M., Vedrenne, G., Kane, S.R., Kouveliotou, C., Cline, T.L., Dennis, B.R., Desai, U.D., Orwig, L.E., Kuznetsov, A.V., Sunyaev, R.A., Terekhov, O.V., 1987, ApJ, 320, L111

[60] Li, X.D., Wang, Z.R., 2000, ApJ, 544, L49

[61] Marsden, D., White, N.E., 2001, ApJ, 551, L155

[62] Marsden, D., Lingenfelter, R.E., Rothschild, R.E., Higdon, J.C., 2001, ApJ, 550, 397

[63] Mazets, E.P., Golenetskii, S.V., Ilinskii, V.N., Aptekar, R.L., Guryan, Iu.A., 1979, Nature, 282, 587

[64] McGarry, M.B., Gaensler, B.M., Ransom, S.M., Kaspi, V.M., Veljkovik, S., 2005, ApJ, 627, L137

[65] McLaughlin, M.A., Stairs, I.H., Kaspi, V.M., Lorimer, D.R., Kramer, M., Lyne, A.G., Manchester, R.N., Camilo, F., Hobbs, G., Possenti, A., D'Amico, N. and Faulkner, A.J., 2003, ApJ, 591, L135

[66] Mereghetti, S., Esposito, P., Tiengo, A., Zane, S., Turolla, R., Stella, L., Israel, G.L., Götz, D., Feroci, M., 2006, ApJ, 653, 1423

[67] Mereghetti, S., Esposito, P., Tiengo, A., Turolla, R., Zane, S., Israel, G.L., Feroci, M., Treves, A., 2006, astro-ph/0512059 v2

[68] Mereghetti, S., Tiengo, A., Esposito, P., Götz, D., Stella, L., Israel, G.L., Rea, N., Feroci, M., Turolla, R., Zane, S., 2005, ApJ, 628, 938

[69] Mereghetti, S., Tiengo, A., Stella, L., Israel, G.L., Rea, N., Zane, S., Oosterbroek, T., 2004, ApJ, 608, 427

[70] Mereghetti, S., Chiarlone, L., Israel, G.L., Stella, L., 2002, Proceedings of the 270. WE-Heraeus Seminer on:"Neutron Stars, Pulsars and Supernova Remnants", eds. W.Becker, H. Lesch & J.Trümper

[71] Mereghetti, S., Cremonesi, D., Feroci, M., Tavani, M., 2000, A&A, 361, 240

[72] Mereghetti, S., Israel, G.L., Stella, L., 1998, MNRAS, 296, 689

[73] Mereghetti, S., Stella, L., 1995, ApJ, 442, L17

[74] Morii, M., Sato, R., Kataoka, J., Kawai, N., 2003, PASJ, 55, L45

[75] Muno, M.P., Clark, J.S., Crowther, P.A., Dougherty, S.M., de Grijs, R., Law, C., McMillan, S.L.W., Morris, M.R., Negueruela, I., Pooley, D., Zwart, S.P., Yusef-Zadeh, F., 2006, ApJ, 636, L41

[76] Oosterbroek, T., Parmar, A.N., Rea, N., Israel, G.L., Stella, L., Meraghetti, S., Haberl, F., Angelini, L., 2004, ESASP, 552, 4710

[77] Özel, F., Güver T., 2007, ApJ, 659, L141

[78] Özel, F., 2002, ApJ, 575, 397

[79] Paczynski, B., 1990, ApJ, 365, L9

[80] Parmar, A.N., Oosterbroek, T., Favata, F., Pightling, S., Coe, M.J., Mereghetti, S., Israel, G.L., 1998, A&A, 330, 175

[81] Paul, B., Kawasaki, M., Donati, T., Nagase, F., 2000, ApJ, 537, 319

[82] Patel, S.K., Kouveliotou, C., Woods, P.M., Tennant, A.F., Weisskopf, M.C., Finger, M.H., Gögüş, E., van der Klis, M., Belloni, T., 2001, ApJ, 563, L45

[83] Patel, S.K., Kouveliotou, C., Woods, P.M., Tennant, A.F., Weisskopf, M.C., Finger, M.H., Wilson, C.A., Gögüş, E., van der Klis, M., Belloni, T., 2003, ApJ, 587, 367

[84] Rea, N., Israel, G.L., Oosterbroek, T., Campana, S., Zane, S., Turolla, R., Testa, V., Mendez, M., Stella, L., 2007, Ap&SS, 308, 505

[85] Rea, N., Tiengo, A., Mereghetti, S., Israel, G.L., Zane, S., Turolla, R., Stella, L., 2005, ApJ, 627, L133

[86] Rea, N., Testa, V., Israel, G.L., Mereghetti, S., Perna, R., Stella, L., Tiengo, A., Mangano, V., Oosterbroek, T., Mignani, R., Curto, G.L., Campana, S., Covino, S., 2004, A&A, 425, L5

[87] Sasaki, M. et al., 2004, ApJ, 617, 322

[88] Shapiro, S.L., Teukolsky, S.A., 1983, John Wiley & Sons

[89] Sonobe, T., Murakami, T., Kulkarni, S.R., Aoki, T., Yoshida, A., 1994, ApJ, 436, L23

[90] Stella, L., Israel, G.L., Mereghetti, S., 1998, Adv. Space Res., 22-7, 1025

[91] Sugizaki, M., Nagase, F., Torii, K., Kinugasa, K., Asanuma, T., Matsuzaki, K., Koyoma, K., Yamauchi, S., 1997, PASJ, 49, L25

[92] Tam, C.R., Kaspi, V.M., Gaensler, B.M., Gotthelf, E.V., 2007, Ap&SS, 308, 519

[93] Tam, C.R., Kaspi, V.M., Gaensler, B.M., Gotthelf, E.V., 2006, ApJ, 652, 548

[94] Tam, C.R., Kaspi, V.M., van Kerkwijk, M.H., Durant, M., 2004, ApJ, 617, L53

[95] Tatematsu, K., Fukui, Y., Nakano, M., Kogure, T., Ogawa, H., Kawabata, K., 1987, A&A, 184,279T

[96] Thompson, C., 2000, astro-ph/0010016 v1

[97] Thompson, C., Duncan, R.C., Woods, P.M., Kouveliotou, C., Finger, M. and van Paradijs, J., 2000, ApJ, 543, 340

[98] Thompson, C., Duncan, R.C., 1996, ApJ, 473, 322

[99] Thompson, C. & Duncan, R.C., 1995, MNRAS, 275, 255

[100] Thompson, C. & Duncan, R.C., 1993, ApJ, 408, 194

[101] Tiengo, A., Esposito, P., Mereghetti, S., Sidoli, L., Götz, D., Feroci, M., Turolla, R., Zane, S., Israel, G.L., Stella, L., Woods,P., 2007, Ap&SS, 308, 33

[102] Tiengo, A., Esposito, P., Mereghetti, S., Rea, N., Stella, L., Israel, G.L., Turolla, R., Zane, S., 2005, astro-ph/0508074 v1

[103] Tiengo, A., Mereghetti, S., Turolla, R., Zane, S., Rea, N., Stella, L., Israel, G.L., 2005, astro-ph/0503390 v1

[104] Tiengo, A., Göhler, E., Staubert, R., Mereghetti, S., 2002, A&A, 383, 182

[105] White, N.E., Angelini, L., Ebisawa, K., Tanaka, Y., Ghosh, P., 1996, 463, L83

[106] White, N.E., Swank, J.H., Holt, S.S., 1983, ApJ, 270, 711

[107] Woods, P.M., Kouveliotou, C., Finger, H. M., Gögüş, E., Colleen, A. W., Patel, K. P., Hurley, Swank, J.H., 2007, ApJ, 654, 470

[108] Woods, P.M., Kouveliotou, C., Gavriil, F.P., Kaspi, V.M., Roberts, M.S.E., Ibrahim, A., Markwardt, C.B., Swank, J.H., Finger, M.H., 2005, ApJ, 629, 985

[109] Woods, P.M., Thompson,C., 2004, astro-ph/0406133 v3

[110] Woods, P.M., Kaspi, V.M., Thompson, C., Gavriil, F.P., Marshall, H.L., Chakrabarty, D., Flanagan, K., Heyl, J., Hernquist, L., 2004, ApJ, 605, 378

[111] Woods, P.M., Kouveliotou, C., Gögüş, E., Finger, H. M., Swank, J.H., Smith, D.A., Hurley, K., Thompson, C., 2001, ApJ, 552, 748

[112] Woods, P.M., Kouveliotou, C., van Paradijs, J., Hurley, K., Kippen, M.R., Finger, H. M., Briggs, M.S., Dieters, S., Fishman, G.J., 1999, ApJ, 519, L139

[113] Woods, P.M., Kouveliotou, C., van Paradijs, J., Finger, H. M., Thompson, C., 1999, ApJ, 518, L103

[114] XTE Technical Appendix, Appendix F, National Aeronautics and Space Administration (NASA), ftp://legacy.gsfc.nasa.gov/xte/nra/appendix-f/, June 2007

[115] van Paradijs, J., Taam, R.E. and van den Heuvel, E.P.J., 1995, A&A, 299, L41